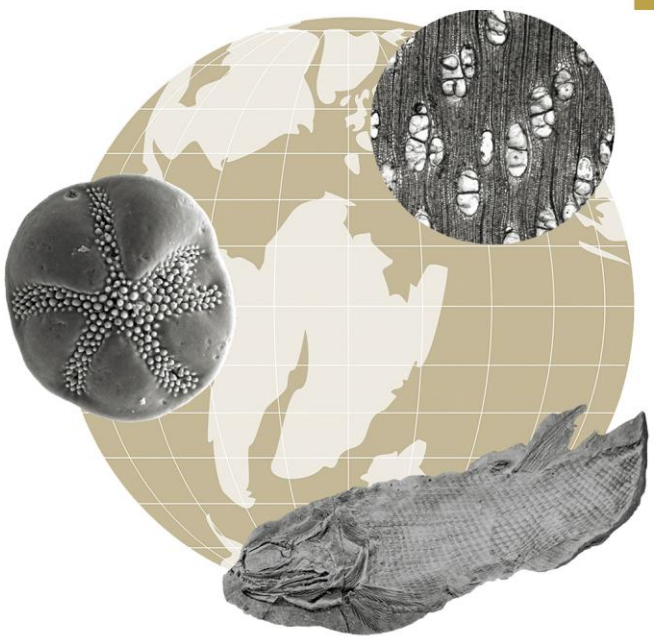
AMEGHINIANA
A GONDWANAN PALEONTOLOGICAL JOURNAL



This file is an uncorrected accepted manuscript (i.e., postprint). Please be aware that this version will change during the production process. This postprint will be removed once the paper is officially published. All legal disclaimers that apply to the journal pertain.

Submitted: 06 July 2026 - **Accepted**: 24 October 2026 - **Posted online**: 27 October 2026

To link and cite this article:

doi: 10.5710/AMGH.24.10.2026.3706

PLEASE SCROLL DOWN FOR ARTICLE

MIOCENE DINOCYST BIOSTRATIGRAPHY AND PALEOENVIRONMENTS OF THE RANQUEL WELL, COLORADO BASIN, ARGENTINA

E. J. Delgado-Kasinsky[1,2*], M. V. Guler[1,2], M. S. González Estebenet[1,2], J. P. Pérez Panera[1,5], E. L. Navarro[3], L. Palazzesi[1,4], Viviana D. Barreda[1,4]

[1] Consejo Nacional de Investigaciones Científicas y Técnicas (CONICET), Argentina

[2] Instituto Geológico del Sur (INGEOSUR), Universidad Nacional del Sur (UNS), San Juan 670, B8000, Bahía Blanca, Buenos Aires, Argentina

[3] Comisión de Investigaciones Científicas (CIC)-CGAMA, Departamento de Geología, Universidad Nacional del Sur (UNS), San Juan 670, B8000, Bahía Blanca, Buenos Aires, Argentina

[4] Sección Paleopalinología, Museo Argentino de Ciencias Naturales "Bernardino Rivadavia", C1405DJR, Buenos Aires, Argentina

[5] División Geología, Museo de La Plata, Facultad de Ciencias Naturales y Museo, Universidad Nacional de La Plata, Paseo del Bosque s/n, B1900FWA, La Plata, Buenos Aires, Argentina

[6] Instituto Patagónico de Geología y Paleontología, CENPAT, Av. Almirante Brown 2915, U9120ACD, Puerto Madryn, Chubut, Argentina

59 pages (text + references); 8 figures; 1 table

Miocene biostratigraphy and paleoeviroments of the offshore Colorado Basin (Ranquel well) based on dinocysts and calcareous nannofossils.

23 Corresponding author: Estefanía Jael Delgado Kasinsky, San Juan 670, 8000 Bahía

24 Blanca, Buenos Aires, estefaniadelgadokasinsky@gmail.com

25

Abstract. The dinocyst assemblages from the YPF.CCMI.Ra es-1 (Ranquel) well, integrated with calcareous nannofossil data, provides a refined biostratigraphic framework and paleoenvironmental reconstruction for the offshore Colorado Basin. A sequence of diagnostic dinocyst events is recognized, including, from oldest to youngest, the highest occurrence (HO) and highest common occurrence (HCO) of *Hystrichokolpoma rigaudiae*, and the HOs of *Cannosphaeropsis quattrocchiae*, *Dapsilidinium pseudocolligerum*, *Labyrinthodinium truncatum*, *Operculodinium piaseckii*, *Trinovantedinium glorianum*, and *Reticulatosphaera actinocoronata*. Based on these events, four stratigraphic intervals are distinguished: an Early Miocene interval correlated with the nannofossil Biozone NN3-NN4; a Middle Miocene interval extending up to the top of the nannofossil Biozone NN6; a Late Miocene interval; and a Late Miocene to Early Pliocene interval. This revised chronology refines the informal palynostratigraphic scheme of the Colorado Basin, indicating that palynozone C ends in the Early Miocene, palynozone B spans the middle to latest Miocene, and palynozone A ranges from the latest Miocene to the Early Pliocene. Quantitative palynological analyses reveal a maximum flooding event during the Early-Middle Miocene, characterized by increased Sea Surface Temperatures (SSTs) and associated with a glacio-eustatic sea level rise during the global warming phase of the Miocene Climatic Optimum (17–14.5 Ma). This interval corresponds to the combined terrestrial and marine palynological assemblages C-T/L and G/C. A subsequent decline of the thermophilic dinocyst taxa, including *Dapsilidinium pseudocolligerum*, *Hystrichokolpoma rigaudiae*, *Operculodinium centrocarpum*, and *Operculodinium janduchenei*, along with the HOs of the calcareous nannofossil genus *Sphenolithus* indicate a progressive decrease of SST related to global cooling since ~14 Ma. Finally, an abrupt continentalization recorded during the latest Miocene − Early Pliocene

reflects a phase of climatic deterioration that may be linked to the earliest documented Late Cenozoic glaciation in Patagonia (7 and 5 Ma).
Keywords. Biostratigraphy. Miocene. Dinocysts. Calcareous nannofossils. Paleoenviroments. Colorado basin.
Resumen. El estudio de las asociaciones de dinoquistes del pozo YPF.CCMI.Ra es-1 (Ranquel), integrado con datos de nanofósiles calcáreos, proporcionó una interpretación bioestratigráfica y paleoambiental para la Cuenca del Colorado costa afuera. Una secuencia de eventos diagnósticos de dinoquistes incluye, del más antiguo al más joven, las ocurrencias más altas (HOs) de *Cannosphaeropsis quattrocchiae*, *Labyrinthodinium truncatum*, *Operculodinium piaseckii*, *Trinovantedinium glorianum* y *Reticulatosphaera actinocoronata*. Se definieron cuatro intervalos estratigráficos: Mioceno Temprano, correlacionado con la Biozona de nanofósiles NN3-NN4; Mioceno Medio, extendiéndose hasta el tope de la Biozona de nanofósiles NN6; Mioceno Tardío; y Mioceno Tardío a Plioceno Temprano. Se ajustó la edad de la zonación informal de la Cuenca del Colorado tal que, la palinozona C termina en el Mioceno Temprano, la palinozona B abarca del Mioceno medio al más tardío, y la palinozona A se extiende desde el Mioceno más tardío hasta el Plioceno Temprano. El análisis palinológico cuantitativo revela un episodio de máxima inundación en el Mioceno Temprano a Medio asociado con un incremento de la temperatura del agua superficial (SSTs), relacionado con un ascenso glacio-eustático del nivel del mar, durante un período de calentamiento global, conocido como Óptimo Climático del Mioceno (17–14.5 Ma). Este intervalo registra las asociaciones palinológicas terrestres y marinas combinadas del Mioceno Temprano C-T/L y G/C. Subsecuentemente, la disminución de los taxones termofílicos *Dapsilidinium pseudocolligerum*, *Hystrichokolpoma rigaudiae*, *Operculodinium centrocarpum* y *Operculodinium janduchenei*, junto con las HOs del

género de nanofósils *Sphenolithus* indican una disminución de la SST relacionada al enfriamiento global que se registra a partir de los ~14 Ma. Una abrupta continentalización registrada durante el Mioceno tardío al Plioceno Temprano coincide con un período de deterioro climático, presumiblemente relacionado con la primera glaciación conocida en Patagonia ocurrida en el Cenozoico Tardío (7 y 5 Ma).
Palabras clave: Bioestratigrafía. Mioceno. Dinoquistes. Nanofósiles Calcáreos. Cuenca del Colorado. Paleoambiente

1. Introduction

The Colorado Basin exhibits the most complete Miocene sedimentary record in the southwestern Atlantic Ocean margin. These deposits are related to the two major marine flooding events that occurred during the Miocene and covered extensive areas of Patagonia (Fig. 1). The older transgressive episode (Early to Middle Miocene) is represented by the subsurface Elvira Formation, mainly composed of glauconitic sandstones, overlaid by the tuff-rich lower Barranca Final Formation (Kaaschieter, 1965), whereas the younger (Middle to Late Miocene) transgression is represented by the upper Barranca Final Formation (Kaaschieter, 1965). The Barranca Final Formation type deposits, composed by clays and sandy clays with occasional tuffaceous intercalations described from the cliffs along the San Matias Gulf margin (Kaaschieter 1963, 1965), constitutes one of the few stratigraphic units cropping out in the Colorado Basin; notably most of the stratigraphic record is confined to the subsurface.

The sedimentary infill of the Colorado Basin (Late Cretaceous – Cenozoic) has been widely analyzed from a palynological perspective (e.g. Ruiz & Quattrocchio, 1997; Pérez Panera *et al*., 2019, Gramerro & Archangelsky, 1971; González Estebenet et al., 2026) and furthermore, during the last decades, advances on organic-walled dinoflagellate cysts (dinocysts) knowledge from exposed and subsurface sections have contributed to the Cenozoic stratigraphy and paleoenvironments of the basin (e.g. Guerstein & Guler, 2000; Guerstein & Junciel, 2001; Guler & Guerstein, 2002; Guler *et al*., 2021; González Estebenet et al., 2026). The present study provides an update of the YPF.CCMI.Ra es-1 (Ranquel) well biostratigraphy, based on the restudy of the dinocysts supported by calcareous nannofossil data. The first study on dinocysts from the Colorado Basin was performed at the YPF.CCMI.Ra es-1 (Ranquel) and YPF. CCMI Pu es-1 (Puelche) wells by Gamerro & Archangelsky (1981), who proposed a

preliminary palynological zonation. The zonation comprises five palynozones informally named, from top to bottom, A to E. In particular, palynozones A, B and C have been widely recognized in deposits related to these Miocene marine events in other wells in the Colorado Basin (Guler *et al.,* 2002; Pérez Panera *et al.*, 2019; Guler *et al*., 2021), as well as in sections of other southwestern Atlantic basins (Parras *et al.*, 2020; Fuentes, 2023; Daners *et al*., 2025).

The revision of dinocysts from the Ranquel x-1 well, using a denser sampling scheme and a larger dataset than the original study, together with taxonomic and biostratigraphic advances achieved during recent decades in Miocene successions of the southwestern Atlantic basins, allowed the development of a high-resolution dinocyst biostratigraphy for the Miocene succession of the well. Furthermore, the integration of palynological and calcareous nannofossil data provided independent age control and supported the recognition and correlation of biostratigraphic events, enabling the refinement of palynological zones A, B, and C proposed by Gamerro and Archangelsky (1981) and the establishment of new age constraints for their boundaries. It is important to note that it represents the only local dinocyst zonation scheme, which has been widely recognized and applied in subsequent studies of the Colorado Basin and neighboring basins (e.g., Guerstein & Guler, 2000; Guler *et al*., 2001; Guler & Guerstein, 2002; Guler *et al*., 2021).

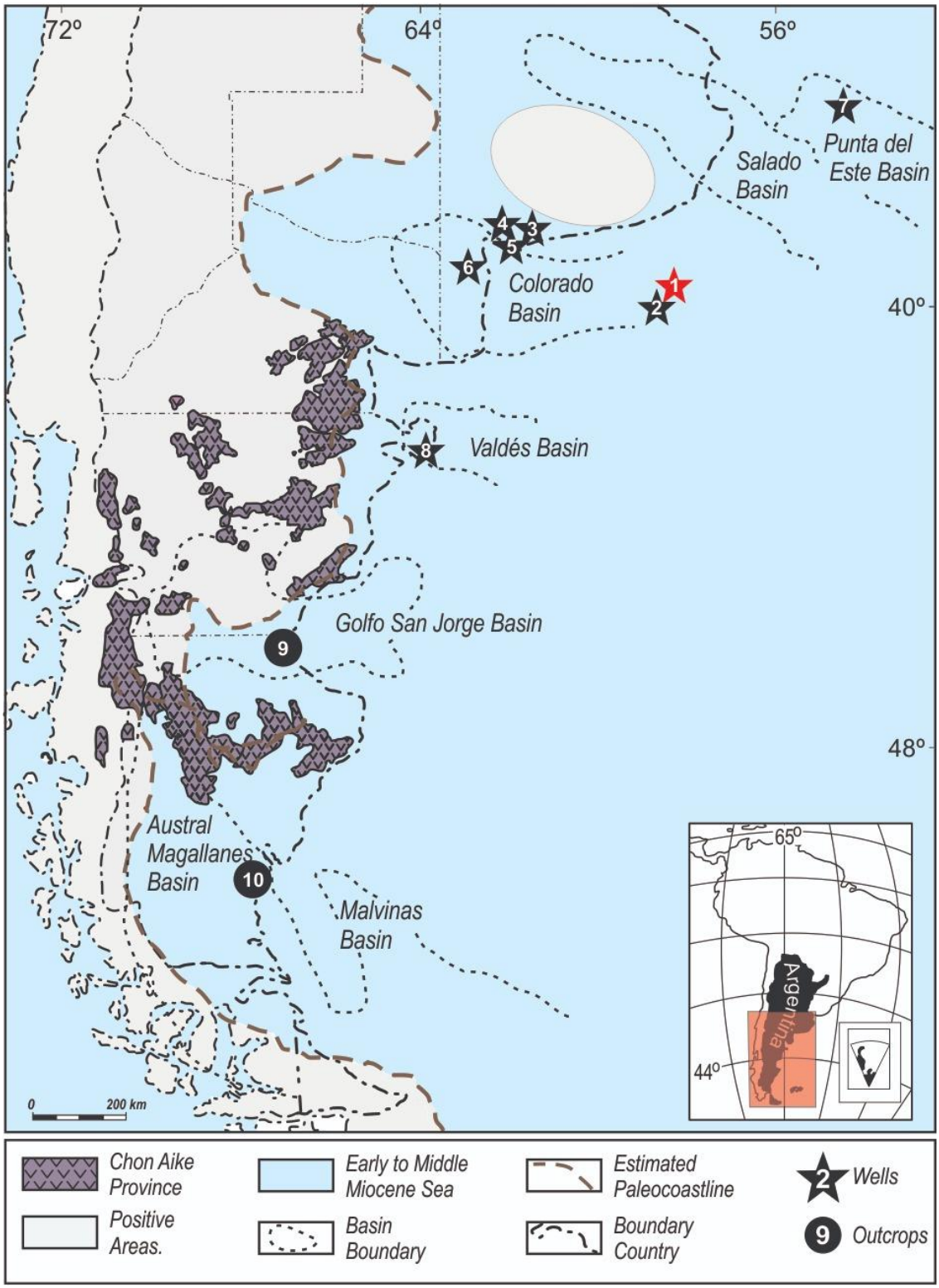


Figure 1. Early to Middle Miocene. Paleogeographic map of the southwestern Atlantic margin, showing the main localities with reported dinocyst occurrences (modified from Malumián & Náñez, 2011; Guler *et al.*, 2021). Colorado Basin: **1.** Ranquel x-1 well (Gamerro & Archangelsky, 1981; this study); **2.** Puelche x-1 well (Gamerro &

Archangelsky, 1981); **3.** Dx-1 well (Guler & Guerstein, 2002); **4.** Fx-1 borehole (Guler & Guerstein, 2002); **5.** Cx-1 well (Guerstein & Junciel, 2001; Guler & Guerstein, 2002); **6.** Ombucta x-1 well (Guerstein & Guler, 2000); Punta del Este basin: **7.** Lobo x-1 (Daners *et al.*, 2025); **8.** Valdés Basin: PV well (Fuentes, 2020; Guler *et al.*, 2021). **9.** Golfo San Jorge Basin: Chenque Formation (Palamarczuk & Barreda, 1998; Barreda & Palamarczuk, 2000a). **10.** Austral Basin: Monte León Formation (Barreda & Palamarczuk 2000b; Parras *et al*., 2012, 2020; Pérez Panera *et al.*, 2014).

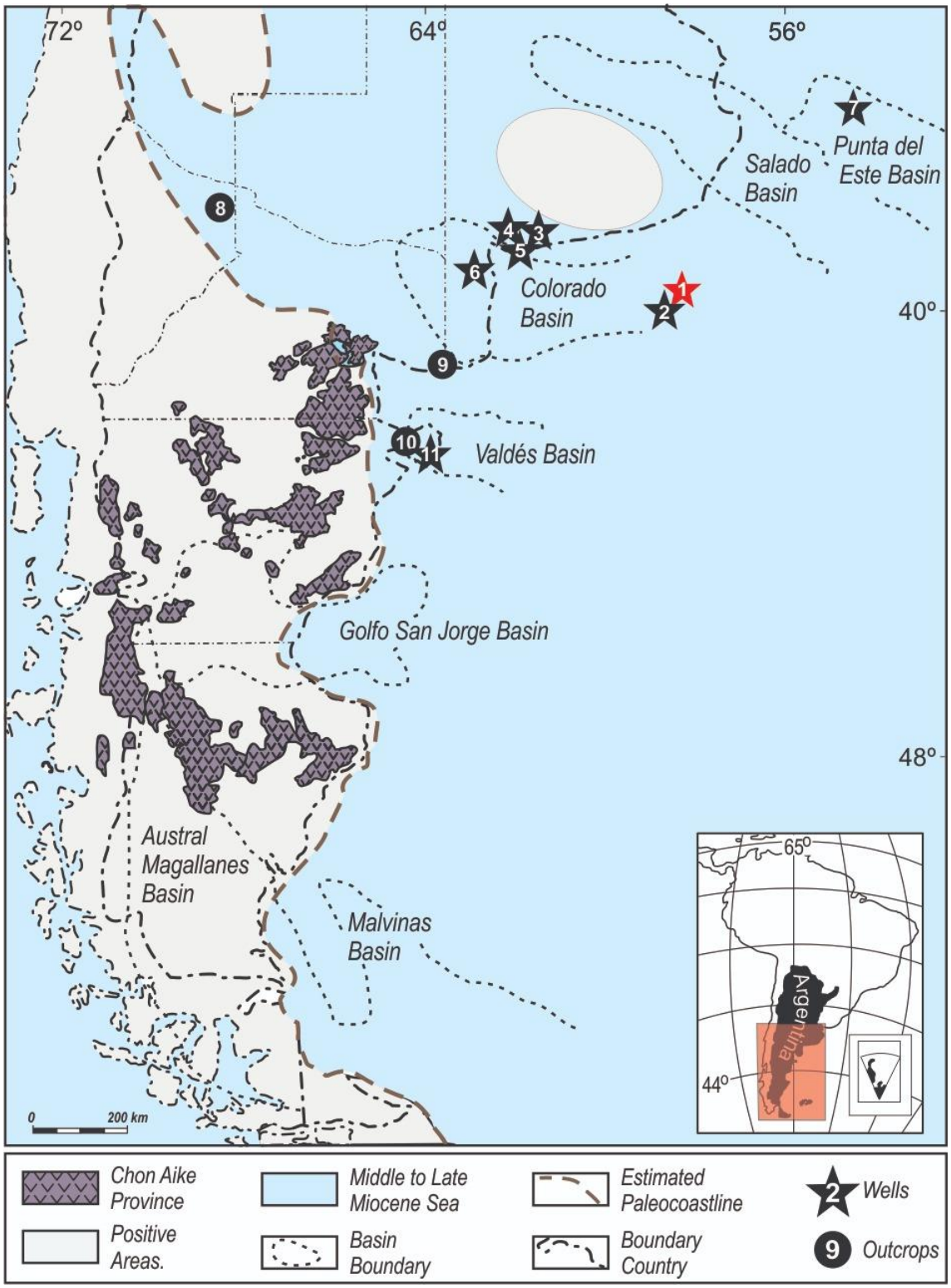


Figure 2. Middle to Late Miocene. Paleogeographic map of the southwestern Atlantic margin showing the main localities with reported dinocyst occurrences (modified from Malumián & Náñez, 2011; Náñez & Malumián, 2019; Guler *et al.*, 2021). Colorado Basin: 1. Ranquel x-1 well (Gamerro & Archangelsky, 1981; this study); 2. Puelche x-1

well (Gamerro & Archangelsky, 1981); 3. Dx-1 well (Guler & Guerstein, 2002); 4. Fx-1 borehole (Guler & Guerstein, 2002); 5. Cx-1 well (Guerstein & Junciel, 2001; Guler & Guerstein, 2002); 6. Ombucta x-1 well (Guerstein & Guler, 2000); 9. Barranca Final Formation type section (Guler *et al.*, 2002; Palazzesi *et al*., 2014; Fuentes *et al.*, 2016), Punta del Este basin: 7. Lobo x-1(Daners *et al*., 2025); 8. Neuquén Basin: Bajada de Añelo region (Nañez & Malumian, 2019); 10–11. Valdés Basin: 10. Puerto Madryn Formation, Valdés Península (Fuentes *et al.*, 2019), 11. PV well (Guler *et al*., 2018; Fuentes, 2020).

2. Geologic framework

The Colorado Basin is located on the southwestern Atlantic margin, primarily situated on the continental shelf between latitudes 38° and 41° S and longitudes 57° and 64° W, covering an area exceeding 160,000 km². Its tectonic origin is linked to an intracratonic rift system developed during the Middle to Late Jurassic, coinciding with the boundary between the South American Craton and the North Patagonian Massif (Uchupi & Emery, 1991; Lovecchio *et al.,* 2018). While the Mesozoic and Cenozoic stratigraphy has been extensively examined by several authors, the tectono-stratigraphic framework identifies three primary units bounded by unconformities and condensed sections: a Late Jurassic to Early Cretaceous syn-rift sequence, followed by an Upper Cretaceous sag stage comprising the Fortín and Colorado formations, and culminating in a drift unit initiated during the Paleocene, which includes the Pedro Luro, Elvira-Ombucta, Barranca Final, and Belén formations (Fryklund *et al.*, 1996). The structural configuration and evolutionary stages of the basin were strongly controlled by three superimposed rifting events, recently integrated into a comprehensive regional model (e.g. Lovecchio *et al.*, 2018, 2024). The tectonic evolution of the basin and the

subsequent opening of the South Atlantic Ocean are documented by major regional seismic and chronostratigraphic unconformities (e.g. Gerster *et al*., 2011; Lovecchio *et al.*, 2024). These tectonic milestones record the transition to the sag stage and the cessation of extension (Mid-Valanginian to Late Hauterivian), accompanied by massive volcanic flows coeval with the Paraná basalts (132 Ma, Menzies *et al.*, 2002).This was followed by the termination of faulting and the initial marine transgression during the Early Aptian, and ultimately, the definitive mechanical separation between the African and South American plates in the Late Aptian, which established the base of the marine platform. The architectural configuration during the Late Cretaceous and the Paleogene transition set the structural framework prior to the fully marine conditions of the Cenozoic (Gerster *et al.*, 2011). Within this regional framework, the Ranquel well represents a critical reference record for the central sector of the Colorado Basin, located offshore approximately 273 km SSE of Mar del Plata. The well, which reached a total depth of 4,466 meters below sea floor (mbsf), is positioned in an outer shelf to upper slope setting and has penetrated a significant sedimentary succession ranging from possible Upper Paleozoic basement rocks to Pliocene deposits. While representing a site-specific succession, the Ranquel well contains a continuous quantitative dinocyst record, which allows for a high-resolution local expression of the paleoenvironmental and paleoclimatic shifts that occurred during the Miocene marine events. This study focuses on the interval between 719 and 1844 mbsf, which corresponds to Miocene marine deposits reflecting a progressive shallowing trend from outer shelf to mid-inner shelf environments, and encompasses the Miocene Climatic Optimum event.

3. Materials and methods

A total of 40 cuttings samples from the YPF.CCMI.Ra es-1 (Ranquel) well, Colorado Basin, from 719 to 1844 mbsf, were analyzed palynologically. Samples were

193 processed using standard palynological procedures, including treatment with
194 hydrochloric (10%) and hydrofluoric (70%) acids for the removal of carbonates and
195 silicates, respectively. Residues were sieved through 10- and 20-µm meshes and
196 mounted using UV-curable acrylates (Trabasil®NR2) as a mounting medium, following
197 the technique described by Noetinger et al. (2017). Additionally, eight samples from
198 selected intervals were processed for calcareous nannofossil analyses, in order to
199 confirm independent age control. These samples were prepared according to the gravity
200 settling technique described in Pérez Panera *et al.* (2023). Transmitted light microscopy
201 was undertaken using a Leica DM 2500, and images were taken with a digital camera
202 MshOt-MSX1. The dinocyst nomenclature overall follows Williams *et al.* (2017). An
203 alphabetical species list of dinocyst taxa is presented in Appendix 1. Stratigraphical
204 distribution of the relative frequencies of the dinocyst taxa was conducted using the
205 Tilia package (Grimm, 1991–1993). Selected specimens of dinocysts are illustrated in
206 Figs. 6-8. The ecological and environmental affinities of the selected dinocyst taxa are
207 presented in Table 1. For the quantitative analysis, more than 500 sedimentary organic
208 matter particles and a minimum of 200 palynomorphs were counted per sample
209 primarily using the 10-µm-sieved residues, supplemented by the 20-µm fraction when
210 necessary; the latter count was used to calculate the terrestrial versus marine
211 palynomorphs ratio (t/m ratio). Separately, to determine dinocyst relative frequencies, a
212 minimum of 250 dinocysts per sample were counted using both the 10- and 20-µm-
213 sieved residues to ensure a statistically representative population. Consequently, eight
214 samples were excluded from the quantitative analyses due to insufficient palynomorph
215 recovery. The sedimentary organic matter components were classified into four main
216 categories: (1) phytoclasts (Phy): translucent, biostructured and opaque,
217 equidimensional or lath-shaped, attributed to woody debris of macrophytes; (2)

218 terrigenous palynomorphs: spores and pollen grains; (3) marine palynomorphs:
219 dinocysts, acritarchs, and foraminiferal linings; and (4) amorphous organic matter
220 (AOM): structureless granular-textured brown masses, derived from the degradation of
221 marine algae. The dissimilarity between the samples in the Ranquel well was compared
222 using Principal Component Analysis (PCA), performed using XLSTAT Software and a
223 correlation matrix (Jolliffe, 2002). The variables used include: (1) warm-water dinocyst
224 taxa (*Melitasphaeridium choanophorum* + *Reticulatosphaera actinocoronata* +
225 D*apsilidinium pseudocolligerum* + *Hytrichokolpoma rigaudiae* + *Operculodinium*
226 *centrocarpum* + *Operculodinium janduchenei*) over total dinocysts, warm-water/d x
227 100, which contribute to reconstructing sea surface temperatures (SST); (2) outer neritic
228 to oceanic dinocyst taxa (*Cannosphaeropsis quattrocchiae* + *H. rigaudiae* +
229 *Nematosphaeropsis rigida*) over total dinocysts, outer neritic to oceanic/d x 100; (3)
230 AOM/(AOM + Phy) ratio, where high values are a signal of reducing, low-oxygenated
231 seafloor conditions (e.g., dysoxia-anoxia) and distal from active sources of terrestrial
232 organic matter; and (4) terrestrial versus marine palynomorphs ratio (t/m ratio), which is
233 a useful parameter to evaluate the influence of terrestrial input, as an indicator of the
234 proximity to the terrestrial source, as well as proximal-distal trends (e.g., Versteegh,
235 1994; Tyson, 1995).
236
237 **Table 1**: Paleoecological affinities of selected dinocyst taxa, after main references.

Primary dinocyst taxa	Primary references	Paleoecological affinities
Impagidinium sp.	Louwey *et al.* (2007), De Schepper & Head (2008)	Occurs in oceanic environments.
Tuberculodinium vancampoae	Head (1996), Marret &	Warm-water preference species. It has been recorded in tropical to subtropical coastal

	Zonneveld (2003), De Schepper *et al.* (2015b), Louwey *et al.* (2007)	sediments between approximately 45°S and 45°N, and is associated with sea surface temperatures (SST) ranging between 16.9 and 36.6.
Reticulatosphaera actinocoronata	Schreck *et al.* (2017), Head (1989)	Warm-water species show broad thermal tolerance, occurring at SSTs between 9 and 25 °C.
Nematosphaeropsis rigida	Marret & Zonneveld (2003), Sluijis *et al.* (2005)	Occurs in oceanic environments.
Habibacysta tectata	Head (1996), De Schepper & Head (2008), Schreck (2012), Louwey *et al.* (2007)	Cool-tolerant species with a thermal range between 8 and 16 °C, showing maximum abundances (over 30%) at SSTs of 10–15 °C.
Bitectatodinium tepikiense	Marret & Zonneveld (2003), Louwey *et al.* (2007), De Schepper *et al.* (2011)	Cool- to temperate-water species typical of fully marine conditions, related to SST between -2 and 21 °C.
Operculodinium janduchenei	Head (1989a), Marret & Zonneveld (2003), Zonneveld, *et al.* (2013)	Occurs in temperate to tropical fully marine environments, within a temperature range of 1–28 °C.
Batiacasphaera minuta	Schreck & Matthiessen (2013)	Occurs in outer-neritic to oceanic environments and is associated with cool- to warm-temperate conditions.
Labyrinthodinium truncatum	Schreck *et al.* (2017)	Associated with warm-water environments, showing a distribution centered at sea surface temperatures (SSTs) between 16 °C and 22 °C, and occasionally occurring at even higher temperatures.
Melitasphaeridium choanophorum	Head (1997), Louwey *et al.* (2007), Price *et al.* (2016), DeSchepper *et al.*	Warm-water species, living in SSTs of 16.6–31.2 °C, with highest abundances around 25–26 °C.

	(2015b), Guler *et al.* (2021)	
Dapsilidinium pseudocolligerum	DeSchepper *et al.* (2015a); Edwards & Andrle (1992); Head (1993, 1996, 1997); Versteegh 1994; De Schepper (2006); De Schepper *et al.*, (2011); Schreck *et al.*, (2017)	Warm-water, (sub)tropical dinocyst, indicating influence of warm Atlantic waters.
Cannosphaeropsis quattrocchiae	Guler *et al.* (2021)	Occurs in outer neritic to oceanic environments.
Hystrichokolpoma rigaudiae	Pross & Brinkhuis (2005), Egger *et al.* (2018) Edwards & Andrle (1992); Head (1993, 1996, 1997); Versteegh 1994; De Schepper (2006); De Schepper *et al.*, (2011); Schreck *et al.*, (2017)	Warm-water species whose abundance decreases during peak glacial conditions, generally indicating outer-neritic to oceanic environments.

4. Results

4.1. Dinocyst assemblages composition and bioevents

A total of 32 (thirty-two) productive samples yielded well preserved palynomorphs. Assemblages are dominated by marine palynomorphs, mainly dinocysts. Other components including terrestrial palynomorphs (pollen grains and spores) and microforaminiferal test linings are subordinate. The stratigraphical

245 distribution of the dinocyst taxa identified are listed in order of their highest
246 occurrences in Table 1 and in alphabetical order in Appendix A. Relative
247 frequencies of dinocyst species, recorded at the Ranquel well, are performed in Fig.
248 3. A succession of diagnostic dinocyst taxa events of local (regional) and global
249 significance was recognized through the analyzed Miocene interval. Dinocyst events
250 are mostly based on the Highest Occurrence (HO) and/or Highest Common
251 Occurrence (HCO) of the taxa, as these assemblages were recovered from cutting
252 samples, and Lowest occurrences (LOs) are susceptible to downhole contamination.
253 Nevertheless, some LOs, which do not present biostratigraphic inconsistency, are
254 discussed here. From youngest to oldest, these bioevents are: the HO of
255 *Reticulatosphaera actinocoronata*, the HO of *Trinovantedinium glorianum*, the HO
256 of *Operculodinium piaseckii*, the HO of *Labyrinthodinium truncatum*, the HO of
257 *Dapsilidinium pseudocolligerum*, the HO of *Cannosphaeropsis quattrocchiae* and
258 the HO and HCO of *Hystrichokolpoma rigaudia*e; all bioevents contribute to the age
259 and environmental interpretation (see 5.1; 5.2). With the exception of the first record
260 of *Trinovantedinium glorianum* in the Colorado Basin, all diagnostic
261 biostratigraphic and/or environmentally-controlled dinocyst taxa events have
262 previously been recorded in other subsurface successions and outcrop sections of the
263 basin. These events therefore constitute useful biostratigraphic markers for
264 correlation both within the Colorado Basin and with coeval deposits in neighboring
265 regions.

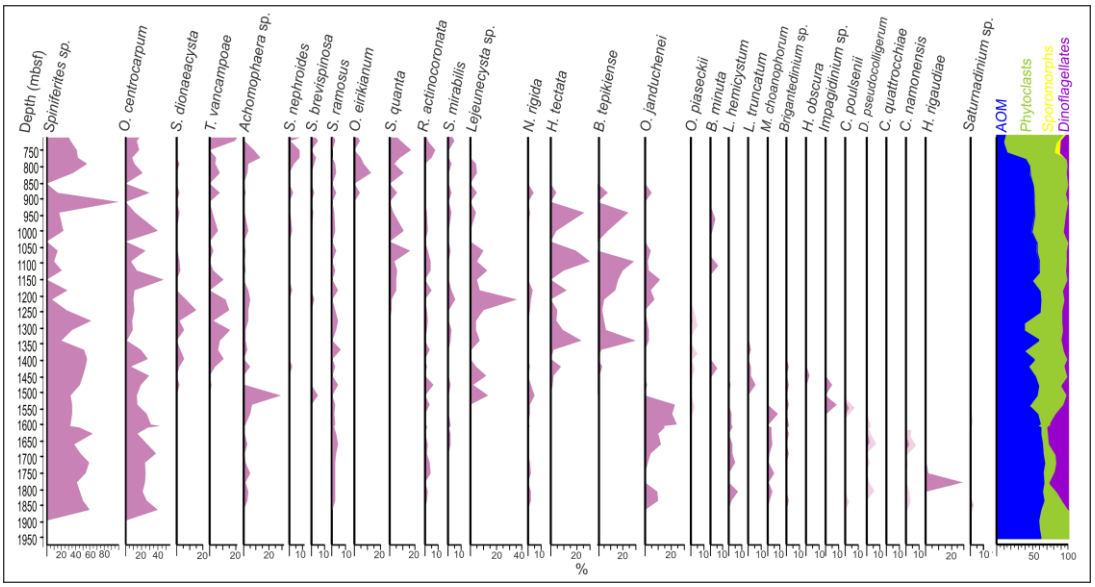


Figure 3. Dinocyst stratigraphical distribution, biostratigraphical intervals and main sedimentary organic matter components identified through the Ranquel well section. (a) Relative frequencies of selected dinocyst taxa. (b) Biostratigraphical intervals I to IV based on dinocysts and nannofossils. (c) Striplog of the percentages of the main categories of the sedimentary organic matter components: Marine-derived amorphous organic matter, phytoclasts, sporomorphs (pollen grain and spores) and dinocysts.

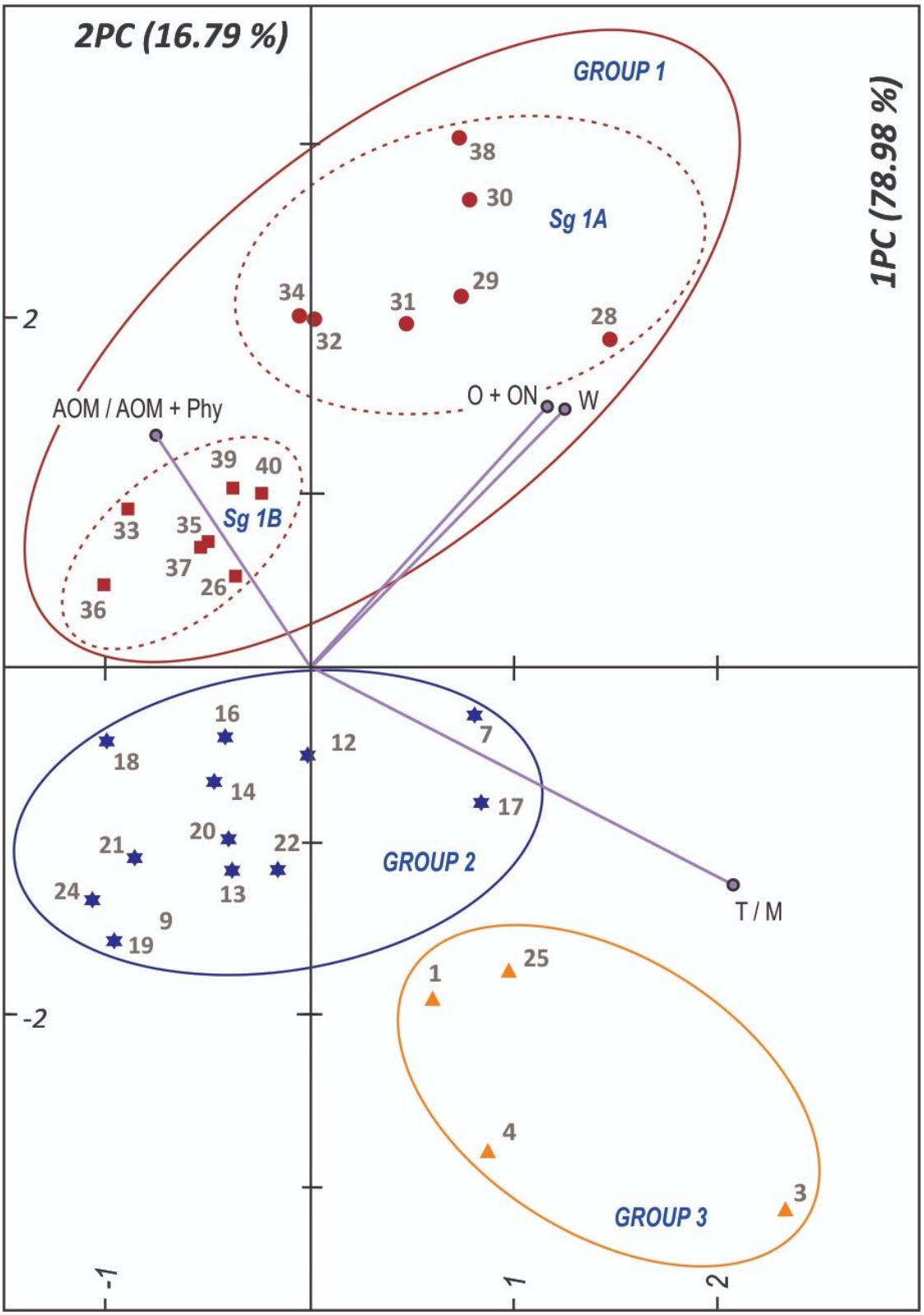
4.2. Quantitative palynological analysis in the Ranquel well

The Principal Component Analysis (PCA) based on 32 selected samples identified three main groups (1 to 3) and two subgroups (1A and 1B) of samples, reflecting distinct environmental and ecological conditions along the Ranquel well in the studied section. The first two Principal Components (1PC and 2PC) (Fig 4) account for 95,8% of the cumulative explained variance. For the 1PC, the variables AOM/(AOM+Phy ratio) (23.0 %), Oceanic + outer neritic taxa (28.3 %) and warm-water taxa (28.9 %) show similar positive contributions, whereas the variable T/M ratio (19.8%) exhibit a negative contribution. For the 2PC, T/M ratio (55.0%) is the variable with the highest positive contribution, along with outer neritic/oceanic taxa (20.0 %) and warm water taxa (17.3%). The AOM/AOM+Phy ratio (7.5%) present negative contribution. Group 1

(two upper quadrants), characterizes the lower part of the section, displays the highest proportions of marine derived components AOM ranging from 45 to 67 % (mean 61%) of total organic matter along with dinocysts proportions between 48.5% and 97.5% (mean 85.5%) of total palynomorphs, whereas phytoclast percentages ranges between 8 – 47 % (mean 19%) and terrestrially-derived palynomorphs are subordinated. Dinocysts are mostly represented by outer neritic to oceanic taxa, along with high proportions of warm water preference taxa. Subgroup 1a differs from subgroup 1b in having the highest proportions of the warm water preference taxa (≥40% of total dinocysts), showing alternating peak abundances (all expressed as % of total dinocysts) of *Operculodinium centrocarpum* (up to 43%), *Operculodinium janduchenei* (up to 29%), *Hystrichokolpoma rigaudiae* (up to 24%) and *Reticulatosphaera actinocoronata* (up to 8%) (Fig. 3). Group 2 (mostly left low quadrant) encompasses the largest number of samples, assemblages denote neritic marine conditions exhibiting abrupt diminishing of outer neritic/oceanic taxa (<13%), associated with a pronounced decline of the warm water taxa (W <30%), along with increase of the terrigenous input (Phy > 31%) of total organic matter). Group 3 represents the highest proportions of the terrestrial derived components (Phy + pollen grains and spores between 45 and 80 %, mean 60%) and the highest T/M ratio (between 0.8 and 4.2).

The representation of 1PC and 2PC individual values of each sample exhibit the environmental changes reflected by the three groups and two subgroups of samples through the YPF.CCMI.Ra es-1 well stratigraphy (Fig. 4). Distal outer neritic to oceanic depositional environments associated with warm sea-surface conditions (Group 1) mark the maximum flooding episode recorded in the lower part of the Miocene analysed section (Fig. 5). Warm sea-surface conditions related to the Burdigalian to Early Langhian maximum flooding episode (Fig. 5) are marked by successive peak

abundances of thermophilic taxa (subgroup 1A) including *H. rigaudiae*, *O. centrocarpum* and *O. janduchenei*. Up section, Group 2 reveals neritic marine conditions associated with a progressive cooling trend, indicated by the disappearance and decline of the warm water preference taxa and the decline of the outer neritic/oceanic taxa during the middle to late Miocene. Finally, Group 3, only represented in the uppermost interval (719/725–791/797 mbsf) as well as at 1448–1457 mbsf in the Ranquel well section, represents the most proximal setting and the seaward migration of the coastline, presumably marking a pronounced shallowing trend and increased continental influence toward the late Miocene and early Pliocene.



317 **Figure 4.** Results of the Principal Component Analysis (PCA) applied to environmental
318 and climatic proxies from the Ranquel well. The biplot illustrates sample scores and
319 variable loadings for axes 1 and 2. The analyzed variables include: the outer neritic-
320 oceanic index (O+ON; oceanic taxa/total dinocysts); the warm-water index (Warm-

water; warm-water taxa/total dinocysts); the terrestrial/marine ratio (t/m); and the amorphous organic matter ratio (AOM/AOM+Phy).

4.3. Calcareous nannofossil assemblages

Calcareous nannofossil assemblages recovered from the analyzed samples are generally sparse and of low diversity, although preservation and abundance vary significantly throughout the succession. The uppermost interval (1244–1425 mbsf) yielded barren samples, consistent with the regressive conditions interpreted for the Tortonian. In the middle part of the section, poorly to moderately diverse assemblages characteristic of the Middle Miocene were identified. Notably, the HO of *Cyclicargolithus floridanus* at 1418–1425 mbsf, marks the top of calcareous nannofossil Biozone NN6 of Martini (1971), indicating a late Serravallian age for the corresponding interval. Other samples from this interval (1508 – 1577 mbsf) contain assemblages compatible with either Langhian or Serravallian ages, although no additional marker species were recorded to refine the age assignment further. Deeper levels yielded progressively more abundant and better-preserved assemblages, including a highly diverse and well-preserved association attributable to the NN3–NN4 interval, supporting a Burdigalian age (sample 1598–1607 mbsf). This interval is also consistent with maximum flooding conditions during the Early Miocene and warmer surface waters due to the presence of species like *Sphenolithus conicus* and *Sphenolithus heteromorphus*. The lowermost analyzed samples yield assemblages of variable preservation and diversity. Sample 1688–1697 mbsf recovered a relatively abundant but low-diversity association dominated by *Reticulofenestra bisecta*, *Reticulofenestra lockeri*, *Reticulofenestra. dictyoda*, *Coccolithus pelagicus*, and *Cyclicargolithus floridanus*, together with scarce thoracosphaerid calcispheres. Although no definitive marker taxa were identified, the

assemblage is broadly consistent with an Early Miocene age, while the presence of indeterminate specimens of *Chiasmolithus* may suggest an age no younger than Oligocene for part of the interval. In contrast, the deepest analyzed samples yielded either extremely poor assemblages composed only of long-ranging taxa or were completely barren.

5. Discussion

5.1. Dinocyst biostratigraphy at the Ranquel well 719–1874 mbsf section

Based on dinocyst events (Figs. 3, 5), we identified four well-defined stratigraphic intervals from 719 to 1874 mbsf. The age of the stratigraphic intervals, from the oldest to the youngest, are: 1. Early Miocene; 2. late Early Miocene to Middle Miocene; 3. early Late Miocene; 4. late Late Miocene to Early Pliocene.

5.1.1. *Interval 1*: *1598–1607 to 1835–1844 mbsf, Early Miocene (Burdigalian)*

The age of the upper part of the interval, from 1598–1607 to 1658–1667 mbsf mainly relies on the stratigraphical range of *Cannosphaeropsis quattrocchiae.* This species is an endemic taxon from the Southwestern Atlantic margin, until now recorded in the Colorado, Valdés, Golfo San Jorge, and Austral basins in Argentina (e.g. Guerstein & Guler, 2000; Guerstein & Junciel, 2001; Guler & Guerstein, 2002; Palamarczuk & Barreda, 1998 (as *C. uttinensis*); Parras *et al*., 2012; Pérez Panera *et al.*, 2014; Parras *et al.*, 2020; Guler et al., 2021) and in the Punta de Este Basin in Uruguay (e.g. Daners *et al.*, 2025). In Patagonia, particularly in the Austral Basin (Monte León Formation, Parras *et al.*, 2012; 2020) and Golfo San Jorge Basin (Chenque Formation, Palamarczuk & Barreda, 1998; Cuitiño *et al.*, 2015), deposits bearing *C. quattrocchiae* were dated between 19.69 and 17.5 Ma. Hence, based on the HO of *C. quattrocchiae*

368 the age of the interval is not younger than Burdigalian. The record of the HO and HCO
369 of the warm-water preference taxa *Hystrichokolpoma rigaudiae* between 1607–1610
370 and 1778–1787 mbsf, respectively, along with the presence of the conspicuous Miocene
371 *Lingulodinium hemicystum* species, points to a Burdigalian age for this part of the
372 interval. The HO and HCO of *H. rigaudiae* invariably occur close to the HO of *C.*
373 *quattrocchiae*, around the Burdigalian and/or the early Langhian in all the subsurface
374 sections analyzed in the Colorado and Valdés basins (e.g. Guler *et al.*, 2021). In
375 addition, the HO of *H. rigaudiae* was recorded in the Burdigalian of the northeastern
376 Punta del Este Basin (e.g. Daners *et al.*, 2025). The early extinction of the species in the
377 Ranquel well supports once again the synchronicity of these bioevents along the
378 southwestern Atlantic basins. As it was interpreted in Guler *et al*., (2021), based on an
379 exhaustive quali- and quantitative analysis, the early extinction of *H. rigaudiae* and *D.*
380 *pseudocolligerum*, seems to be a response of ecological requirement of these taxa,
381 mainly related to paleotemperatures (see section 5.3). The interval records the Early
382 Miocene combined terrestrial and marine palynozones G/C (*Glencopollis ornatus* /
383 *Cannosphaeropsis quattrocchiae*) at the upper part of the interval, and C-T/L
384 (*Cyperaceaepollis neogenicus – Tricolpites*
385 *trioblatus* / *Lingulodinium hemicystum*) at the lower part (Barreda & Palamarczuk,
386 2000). These palynozones are Burdigalian (19.69 – 17.35 Ma) and Burdigalian - earliest
387 Langhian (17.35 – 15.85 Ma) in age, respectively (Barreda & Palamarczuk, 2021).
388 Three basal samples from 1808–1817 to 1835–1844 mbsf do not contain marker
389 dinocyst taxa.
390 In agreement with dinocysts, at 1598–1607 mbsf, a well preserved, abundant and
391 diverse nannofossil assemblage confirms a Burdigalian age for the upper part of this
392 interval. This assemblage is characterized by relatively abundant *Coccolithus pelagicus*,

393 *Cyclicargolithus floridanus*, *Reticulofenestra bisecta* (small forms), *Reticulofenestra*
394 *pseudoumbilicus* and the temperate to warm-water species *Sphenolithus moriformis*,
395 *Sphenolithus heteromorphus* and *Sphenolithus conicus*, among other less represented
396 species. The co-occurrence of *S. conicus*, together with *S. heteromorphus* and
397 *Calcidiscus premacintyrei*, indicates a middle Burdigalian age, in the boundary of NN3
398 and NN4 biozones of Martini (1971). The high abundance and richness of this
399 assemblage, and the presence of temperate to warm-water species, is in agreement with
400 a maximum flooding episode related to the Miocene Climatic Optimum.
401 Sample 1688–1697 mbsf recovered a relatively abundant but low-diversity
402 nannofossil assemblage dominated by *Reticulofenestra bisecta*, *R. lockeri*, *R. dictyoda*,
403 *Coccolithus pelagicus*, and *Cyclicargolithus floridanus*, together with scarce
404 thoracosphaerid calcispheres. Although no definitive marker taxa were identified, the
405 assemblage is broadly consistent with an Early Miocene age, while the presence of
406 indeterminate specimens of *Chiasmolithus* may suggest an age no younger than
407 Oligocene for part of the interval. In contrast, the deepest analyzed samples yielded
408 either extremely poor assemblages composed only of long-ranging taxa or were
409 completely barren. Furthermore, previously reported Eocene indicators from these
410 levels could not be confirmed in the present study, and no supporting evidence was
411 found in the foraminiferal record (e.g. Becker & Bertels 1980; Ronchi *et al.*, 2016;
412 2017). Therefore, the occurrence of Eocene strata in these intervals remains uncertain
413 and may reflect contamination or methodological issues in earlier analyses.
414 **5.1.2.** ***Interval II: 1418–1425 to 1568–1577 mbsf, latest Early Miocene to Middle***
415 ***Miocene (?latest Burdigalian, Langhian to Serravallian)***
416 Based on the HO of *C. quattrocchiae*, the underlying deposits would be not
417 younger than Burdigalian and hence, the overlying interval from 1568–1577 to 1418–

418 1425 may be latest Early Miocene, late Burdigalian (younger than 17,5 Ma; see 5.1.1) to
419 Middle Miocene (Langhian to Serravallian). At 1418–1425 mbsf, the nanofossil species
420 *Cyclicargolithus floridanus*, marks the top of the NN6 Biozone, and indicates an age no
421 younger than late Serravallian (Raffi *et al*., 2006). Below 1508–1517 mbsf, the lower
422 part of the interval, from the HO of *C. quattrocchiae* up to the LO of *Labyrinthodinium*
423 *truncatum* at 1538–1547 mbsf, may indicate proximity to the Burdigalian/Langhian
424 boundary (Fig. 5). The species has the LO around the Early to Middle Miocene
425 boundary (~16 Ma), marking the beginning of the Middle Miocene (e.g. Zevenboom,
426 1995; De Verteuil & Norris, 1996; Strauss *et al.*, 2001; Williams *et al*., 2004; Jimenez-
427 Moreno *et al.*, 2006; Louwye *et al.*, 2008; Soliman, 2012). Assemblages are
428 characterized by peak abundances (HCO) of the warm-water affinity taxa, such as
429 *Melitasphaeridium choanophorum* and *Operculodinium janduchenei*. At the upper part
430 of the interval, assemblages exhibit a marked turnover of species, resulting in
431 assemblages dominated by *Spiniferites* spp. along with the common presence of the
432 cool-tolerant taxa *Habibacysta tectata* and *Bitectatodinium tepikiense* (e.g. Head, 1996;
433 Marret & Zonneveld, 2003; Louwye *et al*., 2007; De Schepper & Head, 2008; De
434 Schepper *et al.*, 2011; Schreck *et al.*, 2012). At 1478–1487 mbsf the LO of *Habibacysta*
435 *tectata* suggests a late Langhian age (14,2 Ma) or younger (e.g. Schreck *et al.*, 2012;
436 Quaijtaal *et al.*, 2014). Moreover, the LO of *Selenopemphix dionaeacysta* at 1478–1487
437 reinforces an age Late Langhian (13,9 Ma; Bijl *et al*., 2022), close to the
438 Langhian/Serravallian boundary.

439 **5.1.3.** ***Interval III: 1244–1250 to 1394–1397mbsf, early Late Miocene (Tortonian).***

440 Above the almost-barren 1394–1397 mbsf interval, and with a separation of 20
441 m, likely involving an unconformity, dinocyst assemblages from the 1244–1250 to
442 1394–1397 mbsf interval exhibit an abrupt turnover of taxa. Assemblages are dominated

by *Spiniferites* spp. (*e.g. S. ramosus*) and *Operculodinium centrocarpum* and the age mainly relies on the marker taxa *Operculodinium piaseckii* and *Labyrinthodinium truncatum.* Calibrated records of *Operculodinium piaseckii* (HO: 8,3 Ma; Shreck *et al.,* 2012; Bijl, 2021) indicates an age no younger than Tortonian for the top of the interval (1244–1250 mbsf). Also, the HO of *Labyrinthodinium truncatum* (1337–1343 mbsf) supports a minimum Tortonian age for the upper part of the interval. In the northern hemisphere, the diagnostic HO event of *L. truncatum truncatum* is between ~7,5 and 8,3 Ma (e.g. Verteuil & Norris, 1996; Donders *et al.*, 2009; Fensome *et al.*, 2009; Dybkjær & Piasecki, 2010; Shreck *et al.*, 2012; Bijl, 2021). In agreement, in the southern hemisphere, from the Barranca Final Formation exposures (Fig. 1) along the northeast coast of Patagonia (Guler *et al.*, 2002), the HO of *L. truncatum* was dated at 8,3 Ma (Palazzesi *et al*., 2014). These outcropping deposits represent the maximum flooding of the Late Miocene marine event in the Colorado Basin (Fuentes *et a*l., 2019; Guler *et al.*, 2021). The HO of *L. truncatum* was identified in other several subsurface sections in the Colorado, Valdés and Punta del Este basins (e.g. Guler *et al.*, 2021; Daners *et al.*, 2025) and related with the late Miocene (Tortonian) Atlantic transgressive event. In the neighboring Valdés Basin, the HO of *L. truncatum* occurs within the maximum flooding/Highstand Phase (e.g. del Río *et al*., 2001; Cuitiño *et al.*, 2017, Fuentes *et al.*, 2019; Guler *et al*., 2021) defined in exposures of the Puerto Madryn Formation in the Peninsula Valdés (Fig. 1), at ~10 Ma (del Río *et al*., 2018), as well as in the subsurface Valdés Basin (Guler *et al*., 2021). Thus, the HO of *L. truncatum* becomes a useful event for long distance (regional) correlation of the Late Miocene (Tortonian) marine deposits, across northeastern Patagonia and the adjacent continental shelf (Fig. 5).

5.1.4. *Interval IV: 719–797 to 1211–1217 mbsf, late Late Miocene (Messinian) to Early Pliocene (Zanclean).*

The HO of *Operculodinium piaseckii* at the base and the HO of *Reticulatosphaera actinocoronata* at the top of the interval suggest an age between the latest Miocene (latest Tortonian and/or Messinian) and Early Pliocene (Zanclean; 4,2 Ma). Also, the dinocyst *Trinovantedinium glorianum* (HO: ~6,3 Ma, Messinian in tropical areas; Cárdenas *et al.*, 2024) shows its HO in the lower part of the interval at 1061–1067 mbsf, which is in accordance to the suggested age span for this interval. The last peak abundance of dinocysts at the maximum sea-level during the Tortonian is followed by the disappearance of a significant number of species, with low diverse and only well representation of the presumed cold-water preference taxa such as *Habibacysta tectata* and *Bitectatodinium tepikiense* (Fig. 3). This shallowing upward pattern with a significant drop in the relative abundance and number of dinocyst species (at most 10 species), is observed in other outcropping and subsurface sections of the Colorado Basin (Guerstein *et al*., 2000; Guerstein & Junciel, 2001; Guler & Guerstein, 2002; Guler *et al.* 2002), as well as in the outcropping Barranca Final section around, 6 Ma (Palazzesi *et al.*, 2014). Furthermore, coetaneous deposits in the neighboring Valdés Basin, dinocyst assemblages were progressively replaced by acanthomorph (micrhystridid) acritarchs in the subsurface YPF.Ch.PV.es-1 (Península Valdés) well section (Guler *et al.*, 2021), whereas at the outcropping Puerto Madryn Formation, phytoplankton assemblages increase the prasinophycean (*Tasmanites*) algae proportions, towards the top of the section (Fuentes *et al.*, 2019), implying in both cases, nearshore environmental conditions.

5.2. Age assessment and index dinocyst events of the Colorado Basin Palynozones A, B and C of Gamerro and Archangelsky (1981)

Based on the restudy of the dinocyst distribution through the Ranquel well, including a denser sampling of the intervals, between 941–947 and 1835–1844 mbsf, we

493 perform a review of the preliminary palynological zonation scheme stated at
494 YPF.CCMI.Ra x-1 (Ranquel) and YPF. CCMI Pu es-1 (Puelche) well by Gamerro and
495 Archangelsky (1981). The authors defined five informal palynozones, named A to E,
496 spanning the Upper Cretaceous (Turonian-Campanian) extending to the Cenozoic (late
497 Miocene). Palynozone A in the Ranquel well was defined based on the analysis of two
498 samples at 600–680 and 680–780 mbsf. The age of the palynozones was not easy to
499 constrain due to the low sampling density, combined with the limited knowledge of
500 dinocyst distribution in the Colorado Basin at that time. So, based on the presence of
501 Asteraceae pollen, the palynozone A was assigned to an Early Miocene age or younger.
502 From our study, the HO of *Reticulatosphaera actinocoronata* at 719–725 mbsf indicates
503 an age not younger than Early Pliocene (Zanclean) close to the top of palynozone A.
504 The HO of *Trinovantedinium glorianum* suggest and age not younger than Messinian
505 for deposits below 1061–1067 mbsf, close to the base of the palynozone A. Hence, the
506 age of palynozone A may be constrained between the Messinian and the early Zanclean.
507 Palynozone B in the Ranquel well spans from 1000 to 1500 mbsf and its base
508 originally assigned to the Oligocene-Miocene boundary, spanning up to the lower and
509 middle Miocene. The HOs of several species at the top of the biozone may be due to the
510 sparse sampling (five samples), since several of those taxa goes into the above
511 palynozone A, *e.g. Tuberculodinium vancampoae*, *Selenopemphix quanta* (as Ciste Tipo
512 51; Lam IV, fig. 6), *Lejeunecysta* spp. (as *Lejeunia* sp. cf. *hyaline*: Lam III, fig. 3 and
513 *Lejeunia* sp. cf. *fallax*: Lam IV, fig. 10 in Gamerro and Archangelsky, 1981). Instead,
514 the HO of *Trinovantedinium glorianum* (as *Spinidinium* cf. *densispinatum*: Lam III, fig.
515 2 in Gamerro and Archangelsky, 1981) at the top of palynozone B, closely coincide
516 with the HO of the species identified in this study at 1061 mbsf. In this sense, the
517 palynozone B may be not younger than Messinian. The HO of *Operculodinium*

518 *piaseckii* at 1244–1250 mbsf and the HO of *Labyrinthodinium trunc*atum at 1337–1343
519 mbsf (this study) would indicate that the lower palynozone B is not younger than
520 Tortonian. Moreover, at 1418–1425 mbsf, the nannofossil species *Cyclicargolithus*
521 *floridanus*, indicates an age not younger than late Serravallian for the lowermost part of
522 the palynozone B.
523 Palynozone C extends from 1500 to around 2050 mbsf, and goes through the
524 upper part of the Ranquel Formation, the Elvira Formation and the base of the Barranca
525 Final Formation. The boundary between the last two units would be at 1740 mbsf
526 (Gamerro & Archangelsky, 1981) and the 500 m-thick interval assigned to the
527 Oligocene (*pars*, lower and middle) and Eocene (*pars*). Following the stratigraphy of
528 the Ranquel well from Lovecchio *et al.* (2018), in this contribution, we analyze the
529 upper part of palynozone C, between 1508–1517 and 1808–1817 mbsf, since deposits
530 around 1820 mbsf, dated at 66±3 Ma by K/Ar ages (Lovecchio *et al.*, 2018), are out of
531 the scope of this study. Anyway, samples between 1835–1844 and 1955–1964 mbsf do
532 not record index taxa, and most are barren of palynomorphs. *Cannosphaeropsis*
533 *quattrocchiae* (as *Cannosphaeropsis* cf. *utinensis*) and *Hystrichokolpoma rigaudiae* (as
534 *Hystrichokolpoma* cf. *rigaudiae*) become extinct around 1500 mbsf, both at the top of
535 the palynozone C. In the present study, and presumably due to a denser sampling, *C.*
536 *quattrocchiae* and *H. rigaudiae* disappear progressively at 1598–1607 and 1607–1610
537 mbsf, respectively. Nevertheless, this difference in the depth of the HOs between the
538 two analyses may not be real, as the sample from the top of palynozone C spans nearly
539 up to 600 mbsf (approximately 100 m), and the HO of *C. quattrocchiae* may well
540 coincide with the HO position recorded in our study. In this way, the HO of *C.*
541 *quattrocchiae* indicate an age not younger than Burdigalian for the top of palynozona C
542 and, moreover, the stratigraphical interval between 1508–1517 to 1658–1667 mbsf,

would represent the lower part of the Barranca Final Formation of Burdigalian age (=Innominado section according to Malumián, 1999), with foraminifera and calcareous nannofossil assemblages comparable to the ones in the Burdigalian Monte León Formation in the Austral Basin (e.g. Malumián, 1999; Parras *et al*., 2020; Pérez Panera *et al.*, 2026). According to Gamerro and Archangelsky (1981), the boundary between the Barranca Final and Elvira Formation at the Ranquel section would be placed at ~1740 mbsf. In dinocyst assemblages from 1748–1757 to 1835–1844 mbsf of the Elvira Formation, we did not record marker species, but we did find the HO of the outer neritic and warm-water preference species *Hystrichokolpoma rigaudiae*. In other subsurface sections in the Colorado and Valdés basins (Guler *et al.*, 2021) and recently, in the Punta del Este Basin (Daners *et al.*, 2025), the HCO of *H. rigaudiae* is invariably linked to the stratigraphic range of *Cannosphaeropsis quattrocchiae,* and therefore, it is inferred to occur within the Burdigalian (see section 5.1,1).

5.3 Miocene maximum flooding episodes and climatic events

During the Cenozoic, successive marine geological events occurred in the Southwestern Atlantic margin (e.g. Uliana & Biddle, 1988; Malumián, 1999; Malumián & Nánez, 2011; Guler *et al.*, 2019, 2021; Navarro *et al.*, 2021; González Estebenet *et al*., 2021, 2025, 2026). Two major transgressive events were recognized during the Miocene, the older during the Burdigalian–earliest Langhian (e.g. Cuitiño *et al*., 2015; Parras *et al.*, 2012) and the latest in the Serravallian – Messinian (e.g. del Río, 1988; del Río *et al*., 2018). In Patagonia, the deposits accumulated during both marine incursions, are informally known ‘Patagoniense’ and ‘Paranense’, consisting of complete marine sedimentary cycles including transgressive and regressive phases (e.g. Cuitiño *et al*., 2017; Guler *et al*., 2021). Moreover, Parras & Cuitiño (2021) defined the *Patagoniense* as a succession of marine sediments accumulated from late Oligocene to early Miocene

(~between 25 and 15 Ma), encompassing different times of accumulation for each basin, including complete stratigraphic cycles of different orders associated with relative sea-level changes. A comprehensive review of the Ranquel well along with a quantitative data analysis allowed us to identify significant biostratigraphical and environmental-driven dinocyst events, useful to constrain in time flooding and climatic episodes occurred in the offshore of the Colorado Basin (Fig. 1).

Our results documented two major palynological changes with important paleoenvironmental implications in the Ranquel well: First, the variables AOM/(AOM+ Phy), (O+ ON) and W show the highest positive contribution to 1PC and points to a maximum flooding episode (Fig. 5). Second, the T/M ratio shows the highest negative contribution to 1PC, marking an abrupt regressive episode characterized by a decline in most of the marine components and an increase in terrestrial derived palynomorphs (highest T/M ratio), denoting increased terrestrial input at the top of the analyzed section. The maximum flooding episode occurred in Early to Middle Miocene (Burdigalian to early Langhian) under warm, oxic to dysoxic, outer neritic to oceanic marine conditions (Figs. 4 and 5). This episode is related to the major Miocene marine event recognized in the southwestern Atlantic basins (e.g. Cuitiño *et al.*, 2017) and correlates with the Patagoniense deposits in Patagonia. The age of this marine event mainly relies on the occurrence of the endemic taxon *Cannosphaeropsis quattrocchiae*, which is calibrated to ~17.5–18.5 Ma (e.g. Cuitiño *et al*., 2015; Parras *et al*., 2012; Pérez Panera *et al*., 2014), and its extinction is close to the maximum flooding at 1598–1607 mbsf at the Ranquel well (Fig. 5). The HO of *C. quatrrocchiae* event is a consistent and isochronous event in several subsurface sections in the Colorado, Valdés and Punta del Este basins (e.g. Guler & Guerstein 2002; Guler *et al*., 2021; Daners *et al.*, 2025). The HO of *C. quattrocchiae* at the Ranquel well constitutes further evidence

593 of the importance of *C. quattrocchiae* as key taxa for regional chronostratigraphic
594 correlation of the Burdigalian successions across the offshore of the southwestern
595 Atlantic basins, as well as with the Lower Miocene marine strata along the east coast of
596 Patagonia. For instance, the well-dated 'Patagoniense' deposits of the Chenque
597 Formation in the Golfo San Jorge Basin; (e.g. Palamarczuk & Barreda, 1998; Barreda &
598 Palamarczuk, 2000a) and the Monte León Formation in the Austral Basin (Parras *et al.*,
599 2012, 2020; Barreda & Palamarczuk, 2000b) and the Gaiman Formation in the Valdés
600 Basin. (e.g. Cuitiño *et al*., 2017, 2019). The distribution of the sedimentation areas of
601 the Patagoniense successions in the in the Magallanes – Austral Basin was mainly
602 driven by global warming and associated global -glacio-eustatic- sea level rise,
603 combined with Andean orogeny influence and associated subsidence (Parras & Cuitiño,
604 2021). Instead, far from the Andean direct orogeny influence, the Cenozoic sedimentary
605 record of the Colorado and Valdés basins might be the result of relatively constant and
606 low subsidence rates, related to non-orogenic processes at the passive margin stage (e.g.
607 Continanzia *et al.*, 2011). In the Ranquel well section, as it was previously observed in
608 the region (e.g. Guler *et al*., 2021), the Early Miocene maximum flooding event is
609 associated with warm sea surface temperatures, presumably related to glacio-eustatic
610 sea level rise (Fig. 5). Alternating peak abundances (expressed as % of total dinocysts)
611 of *Operculodinium centrocarpum* (up to 43%), *Operculodinium janduchenei* (up to
612 29%), *Hystrichokolpoma rigaudiae* (up to 24%) and *Reticulatosphaera actinocoronata*
613 (up to 8%) support relatively high sea surface temperatures (SST) during the
614 Burdigalian to early Langhian in the offshore Colorado Basin, as these taxa are
615 generally considered as indicators of warm-water conditions (e.g., Edwards & Andrle,
616 1992; Head, 1993, 1996, 1997; Versteegh, 1994; De Schepper, 2006; De Schepper *et*
617 *al.*, 2011; Schreck *et al.*, 2017; Egger *et al.*, 2018). The highest relative abundances of

Reticulatosphaera actinocoronata and *Operculodinium centrocarpum* broadly coincide with the modern ecological optima reported for these taxa, associated with relatively warm sea-surface temperatures (above ~18ºC and ~20ºC, respectively; De Schepper et al., 2011; Schreck et al., 2017). However, these values should be regarded as indicative rather than quantitative SST estimates, given that they rely on the ecological affinities of only two taxa and their transferability to a fossil assemblage from a marginal basin remains uncertain (De Schepper *et al*., 2011; Schreck *et al.*, 2017). Furthermore, the HOs of thermophilic taxa such as e.g. *Dapsilidinium pseudocolligerum*, *Hystrichokolpoma rigaudiae* and the HCO *Operculodinium janduchenei* denote a decrease in SST at the southwestern Atlantic margin following the Burdigalian to Langhian interval. Furthermore, *D. pseudocolligerum* and *H. rigaudiae* become extinct next to the HO of *Cannosphaeropsis quattrocchiae*, suggesting both taxa do not extend beyond the Burdigalian to Langhian. As it was observed in other sections along the southwestern Atlantic basins (e.g., Guler *et al.*, 2021; Daners *et al.*, 2025), both species disappear in the early Langhian and the Burdigalian in the Ranquel well, respectively, whereas in the northern hemisphere these taxa persisted longer, ranging into the Pliocene and Pleistocene (e.g. Eberli *et al.*, 1997; Head & Westphal, 1999; Louwye *et al.*, 2004; Fensome *et al.*, 2008; De Schepper *et al.*, 2015). Hence, the early extinction of *Dapsilidinium pseudocolligerum* and *Hystrichokolpoma rigaudiae* denote a strong diachronism between the northern and southern hemispheres. In accordance, calcareous nannofossil assemblages exhibit high species richness and the presence of temperate to warm-water affinity genus taxa like *Sphenolithus* and *Discoaster* (e.g. Pérez Panera *et al.*, 2016; 2019, 2026, this study).

As observed in other sections of the Argentina continental margin basins (e.g. Guler *et al.*, 2021), the early extinction of *D. pseudocollligerum* and *H. rigaudiae*,

643 marked by their HOs and HCOs, may indicate that SST never again became favorable
644 for the proliferation of these thermophilic species in this region of the southwestern
645 Atlantic basins. During the Miocene period, global climate evolved from a prolonged
646 interval of warming that culminated in a Miocene climatic optimum (MCO) between
647 ~17 and ~14 Ma (e.g. Zachos *et al.*, 2001; Holbourn *et al.*, 2013; Westerhold *et al.*,
648 2020), with reduced extent of Antarctic ice. This warm phase was followed by a long-
649 term cooling trend, when the expansion of Antarctic ice-sheet begins, from ~14 Ma (e.g.
650 Shevenell *et al*., 2004; Holbourn *et al*., 2013), resulting in extensive glaciation in both
651 the northern and southern hemispheres, during the Pleistocene (e.g. Zachos *et al.*, 2001).

652 The decline of marine components, including AOM and dinocysts, together with
653 the decrease in abundance and diversity of dinocyst taxa and increased proportions of
654 pollen grains and spores, provides clear evidence of continentalization toward the top of
655 the Ranquel well section analyzed in this study. This abrupt regressive event, which
656 have been regionally recorded across the Colorado and Valdés basins, post Tortonian
657 ages; following a maximum flooding/highstand phase of the Late Miocene marine event
658 during the Tortonian (e.g. Cuitiño *et al*., 2017; del Rio *et al*., 2001; Palazzesi *et al.*,
659 2014; Guler et al., 2021), would coincide with a period of high climatic deterioration
660 with regard to the first known Late Cenozoic Patagonian glaciations occurred between
661 approximately 7 and 5 Ma (Latest Miocene–Earliest Pliocene; Rabassa *et al.*, 2007).
662 This upward continentalization evidenced by the reduction in the abundance of marine
663 fossils and ichnofossils in most of the sections in northeastern Patagonia and across the
664 offshore Colorado and Valdés basin (e.g., del Río *et al.*, 2001; Guler *et al.*, 2002;
665 Cuitiño *et al.*, 2017; Guler *et al.*, 2021) may also correlate with a forced regression
666 recognized at the contact zone between the middle and upper Member of the Rio Negro
667 Formation (e.g. Zavala & Freije, 2000). This sea level -glacio-eustatic- fall, that would

have occurred during post-Tortonian/pre-Early Pliocene age, was compared by some authors with the Mediterranean eustatic fall that originated the so-called Messinian crisis (e.g. Zavala & Freije, 2000).

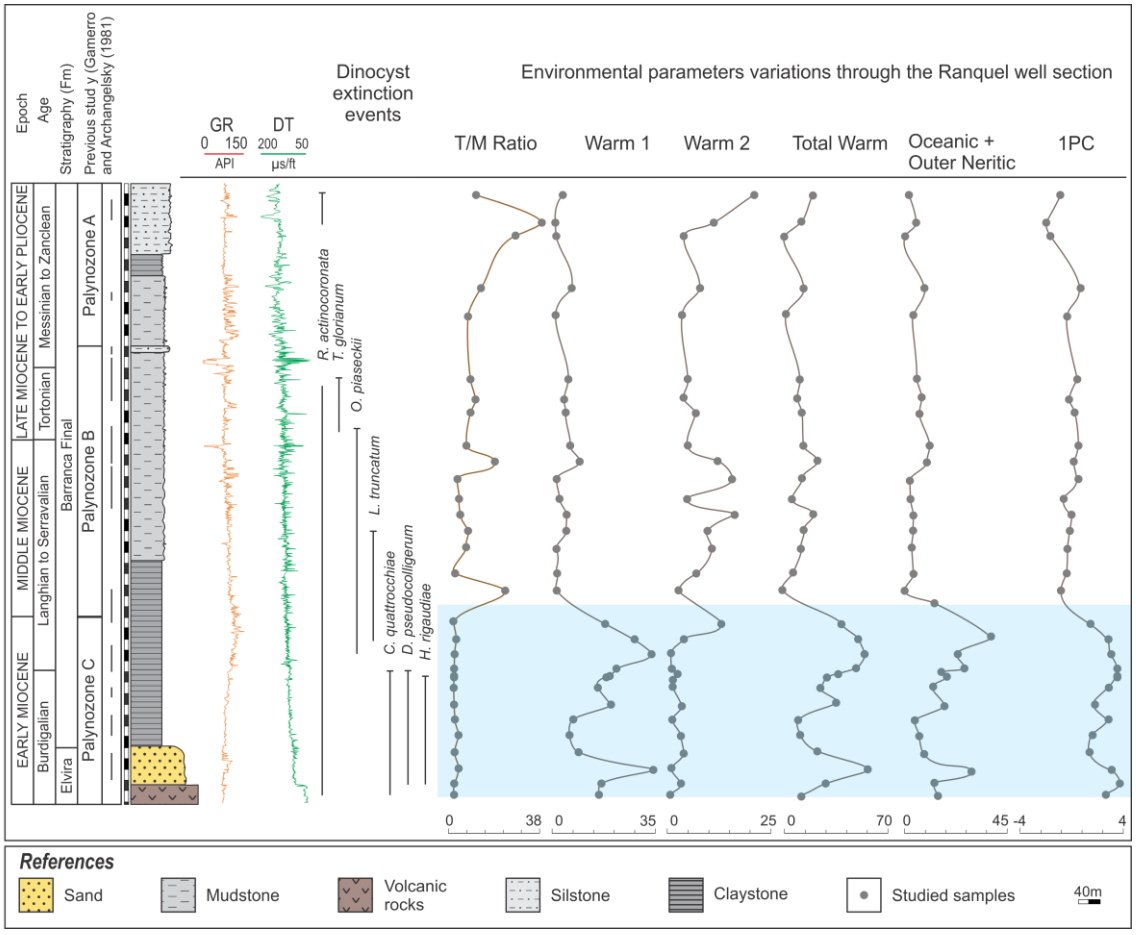


Figure 5. Dinoflagellate cyst and calcareous nannofossil biostratigraphic and palaeoenvironmental reconstructions for the Miocene to Early Pliocene Ranquel well section. (a) Miocene to Early Pliocene dinocyst and calcareous nannofossils extinction events at the Ranquel well. HCO, highest common occurrence. (b) Dinocysts environmental parameters reflect major assemblage turnover around the Early to Middle Miocene and the latest Miocene to Early Pliocene at the Ranquel well section. O+ON: Oceanic + outer neritic dinocyst taxa. W: dinocyst taxa adapted to warm waters. T/M ratio: terrestrial/marine palynomorphs ratio. Palynozones A, B, and C originally defined by Gamerro & Archangelsky (1981), updated with new age assessments. GR: gamma ray log (API units). DT: sonic (delta-T) log (µs/ft).

6. Conclusions

Data from the Ranquel x-1 well reinforces the usefulness of dinocyst events for biostratigraphic and paleoenvironmental interpretations in the offshore Colorado Basin. The Ranquel well exhibits a succession of HOs and HCOs bioevents, from top to bottom (youngest to oldest), are: the HO of *Reticulatosphaera actinocoronata*, the HO of *Trinovantedinium glorianum*, the HO of *Operculodinium piaseckii*, the HO of *Labyrinthodinium truncatum*, the HO of *Dapsilidinium pseudocolligerum*, the HO of *Cannosphaeropsis quattrocchiae*, and the HO and HCO of *Hystrichokolpoma rigaudiae*. The succesion of bioevents occur in the expected stratigraphic order, consistent with the biostratigraphic schemes established for the Colorado and Valdés basins (e.g. Guler *et al.*, 2021). Hence, these bioevents are useful markers for regional correlation in Patagonia as well as in the subsurface of the southwestern Atlantic margin. Dinocyst stratigraphy supported by calcareous nannofossils allowed the identification of four stratigraphic intervals, described here from the youngest to the oldest: Interval 4, late Late Miocene to early Pliocene (Messinian to Zanclean); Interval 3, early Late Miocene (Tortonian); Interval 2, ?latest early Miocene to Middle Miocene (?latest Burdigalian, Langhian to Serravallian); and Interval 1, late early Miocene (Burdigalian).

The taxonomic and biostratigraphic reassessment of the Ranquel well dinocyst assemblages allow refinement of the offshore Colorado Basin zonation scheme established by Gamerro and Archangelsky (1981). The revised age constraints indicate that Palynozone A extends from the Messinian to the early Zanclean, rather than representing early Miocene or younger deposits. Palynozone B is now interpreted to extend into the Late Miocene, spanning the Serravallian-Messinian interval, in contrast to its original placement near the Oligocene / Miocene boundary. The top of Palynozona

706 C coincides with the HO of *C. quattrocchiae*, indicating that this zone does not extend
707 above the Burdigalian.

708 Quantitative palynological analysis of the Ranquel well provides new insight
709 into the paleoclimatic and paleoenvironmental evolution of the offshore Colorado Basin
710 during the Miocene, from warm, well-connected outer-shelf conditions in the early
711 Miocene to progressively more restricted, cooler settings in the younger intervals. A
712 maximum flooding episode, characterized by warm, outer to oceanic (distal) neritic
713 environmental conditions was identified at the Ranquel well, presumably related to
714 glacio-eustatic sea level rise, occurred in the Early to Middle Miocene, Burdigalian –
715 earliest Langhian. A shallowing upward and cooling trend started during the Middle
716 Miocene, related to global cooling and the re-establishments of the Antarctic ice-sheets
717 at ~14 Ma. It culminated at the latest Miocene to early Pliocene, with an abrupt shift
718 from neritic to coastal settings, evidenced by extinction of most marine components,
719 resulting in assemblages composed of a reduced number of species, tentatively
720 coincident with the age range proposed for the first known Late Cenozoic Patagonian
721 glaciations (~7–5 Ma).

722

723 **9. References**

724 Barreda, V. D., & Palamarczuk, S. (2000a). Palinoestratigrafía del Oligoceno tardío-
725 Mioceno, en el área sur del Golfo San Jorge, provincia de Santa Cruz, Argentina.
726 *Ameghiniana*, *37*(1), 103–117.

727 Barreda, V. D., & Palamarczuk, S. (2000b). Palinomorfos continentales y marinos de la
728 Formación Monte León en su área tipo, provincia de Santa Cruz, Argentina.
729 *Ameghiniana*, *37*(1), 3–12.

730 Becker, D., & Bertels, A. (1980). Micropaleontología de la secuencia terciárica de la
731 perforación Puelche (Margen Continental Argentino). *Actas del II Congreso Argentino*
732 *de Paleontología y Bioestratigrafía y I Congreso Latinoamericano de Paleontología*
733 (Vol. 2, pp. 315–333). Buenos Aires.

734 Bijl, P. K. (2022). DINOSTRAT: a global database of the stratigraphic and
735 paleolatitudinal distribution of Mesozoic–Cenozoic organic-walled dinoflagellate cysts.
736 *Earth System Science Data*, *14*(2), 579–617. https://doi.org/10.5194/essd-14-579-2022

737 Bijl, P. K., Guerstein, G. R., Sanmiguel Jaimes, E. A., Sluijs, A., Casadio, S., Valencia,
738 V., Amenábar, C. R., & Encinas, A. (2021). Campanian-Eocene dinoflagellate cyst
739 biostratigraphy in the Southern Andean foreland basin: Implications for Drake Passage
740 throughflow. *Andean Geology*, *48*(2), 185–218. https://doi.org/10.5027/andgeoV48n2-
741 3339

742 Bujak, J. P., Downie, C., Eaton, G. L., & Williams, G. L. (1980). Dinoflagellate cysts
743 and acritarchs from the Eocene of southern England.

744 Cárdenas, D., Rodríguez-Forero, G., Pinzón, D., Vargas, M., Parra, F., & Louwye, S.
745 (2024). The Neogene record of the dinoflagellate cyst genus Trinovantedinium Reid
746 1977 in the tropical Americas. *Review of Palaeobotany and Palynology*, *325*, 105105.
747 https://doi.org/10.1016/j.revpalbo.2024.105105

748 Continanzia, J. C. A., Manceda, R., Covellone, G. M., & Gavarrino, A. S. (2011).
749 Cuencas de Rawson y Valdés: Síntesis del Conocimiento Exploratorio—visión actual.
750 *Simposio Cuencas Argentinas Visión Actual: Actas del VIII Congreso de Exploración y*
751 *Desarrollo de Hidrocarburos* (pp. 47–64). Mar del Plata.

752 Cuitiño, J. I., Fernicola, J. C., Raigemborn, M. S., & Krapovickas, V. (2019).
753 Stratigraphy and depositional environments of the Santa Cruz Formation (early-middle
754 Miocene) along the Río Santa Cruz, southern Patagonia, Argentina.

755 Cuitiño, J. I., Dozo, M. T., del Río, C. J., Buono, M. R., Palazzesi, L., Fuentes, S., &
756 Scasso, R. A. (2017). Miocene marine transgressions: palaeoenvironments and
757 paleobiodiversity. In P. Bouza & A. Bilmes (Eds.), *Late Cenozoic of Península Valdés,*
758 *Patagonia, Argentina* (pp. 47–84). Springer. https://doi.org/10.1007/978-3-319-48508-
759 9_3

760 Cuitiño, J. I., Scasso, R. A., Santos, R. V., & Mancini, L. H. (2015). Sr ages for the
761 Chenque Formation in the Comodoro Rivadavia region (Golfo San Jorge Basin,
762 Argentina): stratigraphic implications. *Latin American Journal of Sedimentology and*
763 *Basin Analysis*, *22*(1), 3–12.

764 Daners, G., Amenábar, C. R., Guerstein, G. R., Pérez Panera, J. P., & Veroslavsky, G.
765 (2025). Maastrichtian to Pliocene dinocyst biostratigraphy of the Lobo X-1 well, Punta
766 del Este Basin, Uruguay. *Journal of South American Earth Sciences*.
767 https://doi.org/10.1016/j.jsames.2025.105796

768 Deflandre, G., & Cookson, I. C. (1955). Fossil microplankton from Australian late
769 Mesozoic and Tertiary sediments. *Marine and Freshwater Research*, *6*(2), 242-314.

770 del Río, C. J., Martinez, S. A., McArthur, J. M., Thirlwall, M. F., & Pérez, L. M.
771 (2018). Dating late Miocene marine incursions across Argentina and Uruguay with Sr-
772 isotope stratigraphy. *Journal of South American Earth Sciences*, *85*, 312–324.
773 https://doi.org/10.1016/j.jsames.2018.05.016

del Río, C. J., Martínez, S. A., & Scasso, R. A. (2001). Nature and origin of spectacular Miocene shell-beds of northeastern Patagonia (Argentina): paleoecological and bathymetric significance. *Palaios*, *16*(1), 3–25. https://doi.org/10.1669/0883-1351(2001)016

De Schepper, S. M. A. (2006). *Plio-Pleistocene dinoflagellate cyst biostratigraphy and palaeoecology of the eastern North Atlantic and southern North Sea Basin* (Doctoral dissertation, University of Cambridge).

De Schepper, S., & Head, M. J. (2008). New dinoflagellate cyst and acritarch taxa from the Pliocene and Pleistocene of the eastern North Atlantic (DSDP Site 610). *Journal of Systematic Palaeontology*, *6*(1), 101–117. https://doi.org/10.1017/S1477201907002167

De Schepper, S., Fischer, E. I., Groeneveld, J., Head, M. J., & Matthiessen, J. (2011). Decoupling of Southern Ocean and North Atlantic surface water dynamics during the Late Miocene. *Paleoceanography*, *26*(4), PA4221. https://doi.org/10.1029/2010PA002061

De Schepper, S., Gibbard, P. L., Salzmann, U., & Ehlers, J. (2015a). A global synthesis of the marine and terrestrial evidence for glaciation during the Pliocene Epoch. *Earth-Science Reviews*, *135*, 83–102. https://doi.org/10.1016/j.earscirev.2014.04.003

De Schepper, S., Schreck, M., Beck, K. M., Matthiessen, J., Fahl, K., & Mangerud, G. (2015b). Early Pliocene onset of modern Nordic Seas circulation related to ocean gateway changes. *Nature Communications*, *6*, 8659. https://doi.org/10.1038/ncomms9659

De Verteuil, L., & Norris, G. (1996). Miocene dinoflagellate stratigraphy and systematics of Maryland and Virginia. *Micropaleontology*, *42*(Supplement 1), 1–172. https://doi.org/10.2307/1485926

Donders, T. H., Weijers, J. W. H., Munsterman, D. K., Kloosterboer-van Hoeve, M. L., Buckles, L. K., Pancost, R. D., ... & Brinkhuis, H. (2009). Strong climate coupling of terrestrial and marine environments in the Miocene of northwest Europe. *Earth and Planetary Science Letters*, *281*(3-4), 215–225. https://doi.org/10.1016/j.epsl.2009.02.034

Dybkjær, K., & Piasecki, S. (2010). Neogene dinoflagellate cyst stratigraphy of the eastern North Sea Basin, Denmark. *Review of Palaeobotany and Palynology*, *161*(1-2), 1–29. https://doi.org/10.1016/j.revpalbo.2010.02.005

Eaton, G. L., Fensome, R. A., Riding, J. B., & Williams, G. L. (2001). Re-evaluation of the status of the dinoflagellate cyst genus Cleistosphaeridium. *Neues Jahrbuch für Geologie und Paläontologie, Abhandlungen*, *219*(1/2), 171-205.

Eberli, G. P., Swart, P. K., Malone, M. J., et al. (1997). *Proceedings of the Ocean Drilling Program, Initial Reports* (Vol. 166). Ocean Drilling Program.

Edwards, L. E., & Andrle, V. A. S. (1992). Distribution of selected dinoflagellate cysts in modern marine sediments. In M. J. Head & J. H. Wrenn (Eds.), *Neogene and Quaternary Dinoflagellate Cysts and Acritarchs* (pp. 259–288). American Association of Stratigraphic Palynologists Foundation.

Egger, L. M., Bahr, A., Friedrich, O., Wilson, P. A., Norris, R. D., van Peer, T. E., ... & Pross, J. (2018). Sea-level and surface-water change in the western North Atlantic

across the Oligocene–Miocene transition: A palynological perspective from IODP Site U1406 (Newfoundland margin). *Marine Micropaleontology*, *139*, 57–71. https://doi.org/10.1016/j.marmicro.2017.11.003

Fensome, R. A., MacRae, R. A., & Williams, G. L. (2008). DINOFLAJ2000: a database of modern and fossil dinoflagellates. *AASP Contributions Series*, *42*.

Fensome, R. A., Williams, G. L., & MacRae, R. A. (2009). Late Cretaceous and Cenozoic fossil dinoflagellates and other palynomorphs from the Scotian Margin, offshore eastern Canada. *Journal of Systematic Palaeontology*, *7*(1), 1–79.

Fryklund, B., Marshall, A., & Stevens, J. (1996). Cuenca del Colorado. In V. A. Ramos & M. A. Turic (Eds.), *Geología y Recursos Naturales de la Plataforma Continental Argentina. Relatorio del XIII Congreso Geológico Argentino y III Congreso de Exploración de Hidrocarburos* (pp. 135–158). Buenos Aires.

Fuentes, S. (2023). Miocene dinoflagellate cyst biostratigraphy of the Península Valdés, Patagonia, Argentina. *Palynology*, *47*(4), 2212276. https://doi.org/10.1080/01916122.2023.2212276

Fuentes, S. N., Cuitiño, J. I., Martz, P., Pérez Panera, J. P., Guler, M. V., Palazzesi, L., & Scasso, R. A. (2019). Palaeoenvironmental reconstruction of the Puerto Madryn Formation (middle to late Miocene), northeast of Patagonia: palynology, nannofossils and stratigraphy. *Ameghiniana*, *56*(1), 28–52. https://doi.org/10.5710/AMGH.11.12.2018.3201

Fuentes, S. N., Guler, M. V., Cuitiño, J. I., Palazzesi, L., Scasso, R. A., & Barreda, V. D. (2016). Bioestratigrafía basada en quistes de dinoflagelados del Neógeno en el

noreste de la Patagonia, Argentina. *Revista Brasileira de Paleontologia*, *19*(2), 303–314. https://doi.org/10.4072/rbp.2016.2.12

Gamerro, J. C., & Archangelsky, S. (1981). Palinozonas neocretácicas y terciarias de la plataforma continental argentina en la Cuenca del Colorado. *Revista Española de Micropaleontología*, *13*(1), 119–140.

Gerster, R., Welsink, H., Ansa, A., & Raggio, F. (2011). Cuenca de Colorado. *Simposio Cuencas Argentinas. Actas del VIII Congreso de Exploración y Desarrollo de Hidrocarburos* (pp. 65–80). Mar del Plata.

González Estebenet, M. S., Guler, M. V., Navarro, E. L., Palazzesi, L., Barreda, V. D., Pérez Panera, J. P., & Caramés, A. (2025). Biostratigraphy, paleoenvironment and paleoclimate in northeastern Patagonia during the early Paleocene based on the micropaleontological record. *Evolving Earth*, *3*, 100052. https://doi.org/10.1016/j.eve.2024.100052

González Estebenet, M.S., Guler, M.V., Vellekoop, J., Navarro, E.L., Palazzesi, L., Kasinsky, E.D., Panera, J.P.P. and Barreda, V.D., 2026. Dinocyst biostratigraphic framework from the Maastrichtian to Danian at Southern Hemisphere Mid-Latitudes, Argentina. Marine Geoscience and Energy Resources, p.207832.

González Estebenet, M. S., Guler, M. V., & Pérez Panera, J. P. (2021). Late Maastrichtian to Danian organic-walled dinoflagellate cysts and calcareous nannofossils from eastern Austral Basin, Patagonia, Argentina. *Review of Palaeobotany and Palynology*, *287*, 104342. https://doi.org/10.1016/j.revpalbo.2020.104342

Guerstein, G. R., & Guler, M. V. (2000). Bioestratigrafía basada en quistes de dinoflagelados del Eoceno-Mioceno del pozo (YPF) Ombucta x-1, Cuenca del Colorado, Argentina. *Ameghiniana*, *37*(1), 81–90.

Guerstein, G. R., & Junciel, G. L. (2001). Quistes de dinoflagelados del Cenozoico de la Cuenca del Colorado, Argentina. *Ameghiniana*, *38*(3), 299–316.

Guler, M. V., González Estebenet, M. S., & Fuentes, S. (2018). *Informe Bioestratigráfico del Pozo YPF-Ch-PV. es-1 (Península de Valdés) basado en quistes de dinoflagelados* (Y-TEC Internal Report, Unpublished).

Guler, M. V., González Estebenet, M. S., Navarro, E. L., Astini, R. A., Pérez Panera, J. P., Ottone, E. G., Pieroni, D., & Paolillo, M. A. (2019). Maastrichtian to Danian Atlantic transgression in the north of Patagonia: a dinoflagellate cyst approach. *Journal of South American Earth Sciences*, *92*, 552–564. https://doi.org/10.1016/j.jsames.2019.04.002

Guler, M. V., González Estebenet, M. S., Navarro, E. L., Fuentes, S., Cuitiño, J. I., Palazzesi, L., Pérez Panera, J. P., & Barreda, V. D. (2021). Miocene Atlantic transgressive-regressive events in northeastern and offshore Patagonia: a palynological perspective. *Journal of South American Earth Sciences*, *109*, 103239. https://doi.org/10.1016/j.jsames.2021.103239

Guler, M. V., & Guerstein, G. R. (2002). Bioestratigrafía del Oligoceno–Plioceno temprano de la Cuenca del Colorado (Argentina) basada en quistes de dinoflagelados. *Revista Española de Micropaleontología*, *34*(3), 359–371.

Guler, M. V., Guerstein, G. R., & Malumián, N. (2002). Bioestratigrafía de la Formación Barranca Final, Neógeno de la Cuenca del Colorado, Argentina. *Ameghiniana*, *39*(1), 103–110.

Guler, M. V., Guerstein, G. R., & Quattrocchio, M. E. (2001). Palinología del Neógeno de la perforación Cx-1, Cuenca del Colorado, Argentina. *Revista Española de Micropaleontología*, *33*(2), 183–204.

Head, M. J. (1993). Dinoflagellate cysts, sporomorphs, and other palynomorphs from the marine uppermost Pliocene St. Erth Beds, Cornwall, southwestern England. *Paleontological Society Memoir*, *31*, 1–62.

Head, M. J. (1996). Late Cenozoic dinoflagellates from the Royal Society borehole at Ludham, Norfolk, eastern England. *Journal of Paleontology*, *70*(4), 543–570. https://doi.org/10.1017/S0022336000023532

Head, M. J. (1997). Thermophilic dinoflagellate assemblages from the mid-Pliocene of eastern England. *Journal of Paleontology*, *71*(2), 165–193. https://doi.org/10.1017/S0022336000039123

Head, M. J., Norris, G., & Mudie, P. J. (1989). New species of dinocysts and a new species of acritarch from the upper Miocene and lowermost Pliocene, ODP Leg 105, Site 646, Labrador Sea. *Proceedings of the Ocean Drilling Program, Scientific Results*, *105*, 453–466. https://doi.org/10.2973/odp.proc.sr.105.136.1989

Head, M. J., & Westphal, H. (1999). Palynology and paleoenvironments of a Pliocene carbonate platform: the Clino Core, Bahamas. *Journal of Paleontology*, *73*(1), 1–25.

902 Holbourn, A., Kuhnt, W., Clemens, S., Prell, W., & Andersen, N. (2013). Middle to late
903 Miocene stepwise climate cooling: Evidence from a high-resolution deep water isotope
904 curve spanning 8 million years. *Paleoceanography*, *28*(4), 688–699.
905 https://doi.org/10.1002/palo.20053

906 Jiménez-Moreno, G., Head, M. J., & Harzhauser, M. (2006). Early and Middle Miocene
907 dinoflagellate cyst stratigraphy of the Central Paratethys, Central Europe. *Journal of*
908 *Micropalaeontology*, *25*(2), 113–139.

909 Jolliffe, I. T. (2002). Graphical representation of data using principal components.
910 *Principal Component Analysis* (pp. 78–110). Springer.

911 Kaasschieter, J. P. H. (1963). Geology of the Colorado basin. *Tulsa Geological Society*
912 *Digest*, *31*, 177–187.

913 Kaasschieter, J. P. H. (1965). Geología de la Cuenca del Colorado. *Actas de las*
914 *Segundas Jornadas Geológicas Argentinas*, *3*, 251–269. Salta.

915 Louwye, S., De Schepper, S., Laga, P., & Vandenberghe, N. (2007). The Upper
916 Miocene of the southern North Sea Basin (northern Belgium): A palaeoenvironmental
917 and stratigraphical reconstruction using dinoflagellate cysts. *Geological Magazine*,
918 *144*(1), 43–52. https://doi.org/10.1017/S0016756806002627

919 Louwye, S., Foubert, A., Mertens, K., & Van Rooij, D. (2008). Integrated stratigraphy
920 and palaeoecology of the lower and middle Miocene of the Porcupine Basin. *Geological*
921 *Magazine*, *145*(3), 321–344. https://doi.org/10.1017/S0016756807004244

Louwye, S., Head, M. J., & De Schepper, S. (2004). Dinoflagellate cyst stratigraphy and palaeoecology of the Pliocene in northern Belgium, southern North Sea Basin. *Geological Magazine*, *141*(3), 353–378. https://doi.org/10.1017/S0016756804009136

Lovecchio, J. P., Abdelmalak, M. M., Planke, S., Silio, O., Rohais, S., Arismendi, S., Rojas Vera, E., Kulhanek, D. K., Bolatti, N., & Ramos, V. A. (2024). Mesozoic Rifting in SW Gondwana and Breakup of the Southern South Atlantic Ocean. *Geological Society, London, Special Publications*, *547*, 75–107. https://doi.org/10.1144/SP547-2023-140

Lovecchio, J. P., Rohais, S., Joseph, P., Bolatti, N., Kress, P., Gerster, R., & Ramos, V. A. (2018). Multistage rifting evolution of the Colorado basin (offshore Argentina): Evidence for extensional settings prior to the South Atlantic opening. *Terra Nova*, *30*(5), 359–368.

Malumián, N. (1999). La sedimentación y el volcanismo terciarios en la Patagonia extraandina. In R. Caminos (Ed.), *Geología Argentina* (Anales 29, pp. 557–578). Instituto de Geología y Recursos Minerales.

Malumián, N., & Náñez, C. (2011). The Late Cretaceous–Cenozoic transgressions in Patagonia and the Fuegian Andes: foraminifera, palaeoecology, and palaeogeography. *Biological Journal of the Linnean Society*, *103*(2), 269–288. https://doi.org/10.1111/j.1095-8312.2011.01649.x

Marret, F., & Zonneveld, K. A. F. (2003). Atlas of modern organic-walled dinoflagellate cyst distribution. *Review of Palaeobotany and Palynology*, *125*(1-2), 1–200. https://doi.org/10.1016/S0034-6667(02)00229-4

Martini, E. (1971). Standard Tertiary and Quaternary calcareous nannoplankton zonation. In A. Farinacci (Ed.), *Proceedings of the II Planktonic Conference, Roma 1970* (Vol. 2, pp. 739–785). Edizioni Tecnoscienza.

Náñez, C., & Malumián, N. (2019). Foraminíferos miocenos en la Cuenca Neuquina, Argentina: implicancias estratigráficas y paleoambientales. *Andean Geology*, *46*(1), 183–210. https://doi.org/10.5027/andgeov46n1-3142

Navarro, E. L., González Estebenet, M. S., Guler, M. V., Fuentes, S., Cuitiño, J. I., Palazzesi, L., Pérez Panera, J. P., & Barreda, V. D. (2021). Environmental variables database in a Miocene marine stratigraphical section: Multivariate statistical analysis. *Data in Brief*, *37*, 106975. https://doi.org/10.1016/j.dib.2021.106975

Noetinger, S., Pujana, R. R., Burrieza, A., & Burrieza, H. P. (2017). Use of UV-curable acrylates gels as mounting media for palynological samples. *Revista del Museo Argentino de Ciencias Naturales*, *19*(1), 19-23.

Palamarczuk, S., & Barreda, V. D. (1998). Bioestratigrafía en base a quistes de dinoflagelados de la Formación Chenque (Mioceno), provincia del Chubut, Argentina. *Ameghiniana*, *35*(4), 415–426.

Palazzesi, L., Barreda, V. D., Cuitiño, J. I., Guler, M. V., Tellería, M. C., & Santos, R. V. (2014). Fossil pollen records indicate that Patagonian desertification was not solely a consequence of Andean uplift. *Nature Communications*, *5*, 3558. https://doi.org/10.1038/ncomms4558

Parras, A., Dix, G. R., & Griffin, M. (2012). Sr-isotope chronostratigraphy of Paleogene/Neogene marine deposits: Austral Basin, southern Patagonia (Argentina).

Journal of South American Earth Sciences, *37*, 122–135. https://doi.org/10.1016/j.jsames.2012.02.007

Parras, A., Guerstein, G. R., Pérez Panera, J. P., Griffin, M., Náñez, C., Cusminsky, C., & Quiroga, A. (2020). Integrated stratigraphy and paleontology of the lower Miocene Monte León Formation, southeastern Patagonia, Argentina: unraveling paleonvironmental changes and factors controlling sedimentation. *Palaeogeography, Palaeoclimatology, Palaeoecology*, *558*, 109701. https://doi.org/10.1016/j.palaeo.2020.109701

Parras, A., & Cuitiño, J. I. (2021). Revised chrono and lithostratigraphy for the Oligocene-Miocene Patagoniense marine deposits in Patagonia: Implications for stratigraphic cycles, paleogeography, and major drivers. *Journal of South American Earth Sciences*, *110*, 103327.

Pérez Panera, J. P., Angelozzi, G. N., Riccardi, C. A., Damborenea, S. C., & Manceñido, M. O. (2023). Late Triassic calcareous nannofossil from Arroyo Malo Formation, Neuquén Basin, Argentina. Implications for their early evolution and dispersal. *Ameghiniana*, *60*(2), 149–163.

Pérez Panera, J. P., Calvo Marcilese, L., Pisano, F., Carignano, A. P., & Cusminsky, G. C. (2026). Neogene to Holocene calcareous microfossils record in the Pampean region: insights into climate and paleoenvironmental evolution. In G. Gasparini, J. Rabassa, & E. P. Tonni (Eds.), *Geology, Stratigraphy, Biostratigraphy, Palaeoenvironments and Climatology of the South American Pampas* (pp. 183–212). Springer.

Pérez Panera, J. P., Guerstein, G. R., Heredia, E., Parras, A., Griffin, M., & Paez, M. (2014). Calcareous nannofossils, palynological and sedimentological data from the early

Miocene Monte León Formation and the lowermost Santa Cruz Formation, southern Patagonia, Argentina. In *Actas del 4th International Palaeontological Congress* (CD-ROM). Mendoza.

Pérez Panera, J. P., Ronchi, D. I., Angelozzi, G., Calvo Marcilese, L., Tórtora, L., Calaramo, N., Lovecchio, J. P., & Kress Frieling, P. R. (2016). Late Cretaceous – Cenozoic biostratigraphy and palaeoenvironmental reconstruction of the Salado and Punta del Este Basins, Southwestern Atlantic Ocean. *Actas del 11° Congreso de la Asociación Paleontológica Argentina* (p. 132). General Roca.

Pérez Panera, J. P., Ronchi, D. I., Angelozzi, G. N., Lovecchio, J. P., Calvo Marcilese, L., Hiriart, M. L., Tórtora, L., Calaramo, N., Cuciniello, C. D., & Ottone, E. G. (2019). Biostratigraphy and Palaeoenvironmental evolution of the Colorado Basin, South Atlantic Ocean. *AAPG International Conference and Exhibition (ICE)*. Buenos Aires.

Price, A. M., Baustian, M. M., Turner, R. E., Rabalais, N. N., & Chmura, G. L. (2016). *Melitasphaeridium choanophorum* – a living fossil dinoflagellate cyst in the Gulf of Mexico. *Palynology*, *41*(3), 361–368. https://doi.org/10.1080/01916122.2016.1205676

Pross, J., & Brinkhuis, H. (2005). Organic-walled dinoflagellate cysts as paleoenvironmental indicators in the Paleogene; a synopsis of concepts. *Paläontologische Zeitschrift*, *79*(1), 53–59. https://doi.org/10.1007/BF03021753

Quaijtaal, W., Donders, T. H., Persico, D., & Louwye, S. (2014). Characterising the middle Miocene climatic optimum: dinoflagellate cyst and acritarch assemblages from the eastern North Atlantic (Porcupine Basin). *Review of Palaeobotany and Palynology*, *206*, 49–67. https://doi.org/10.1016/j.revpalbo.2014.01.006

1011 Rabassa, J., Coronato, A., & Salemme, M. (2007). Chronology of the Late Cenozoic
1012 Patagonian glaciations and their correlation with biostratigraphic units of the Pampean
1013 region (Argentina). *Journal of South American Earth Sciences*, *20*(1-2), 81–103.

1014 Raffi, I., Backman, J., Fornaciari, E., Pälike, H., Rio, D., Lourens, L., & Hilgen, F.
1015 (2006). A review of the 136 stratigraphic principles of the calcareous nannofossil
1016 stratigraphy and the Cenozoic global standard zonation. *Marine Micropaleontology*,
1017 *58*(3), 209–236.

1018 Ronchi, D.I., Pérez Panera, J.P., Ottone, G. 2017. Estudio Bioestratigráfico y
1019 Paleoambiental del Pozo BB-B.x-1 (Bahía Blanca), Cuenca del Colorado. Internal
1020 report. YPF Tecnología SA. pp. 63.

1021 Ronchi, D.I., Angelozzi, G.N., Pérez Panera, J.P. 2016. Revisión Bioestratigráfica y
1022 Paleoambiental del Pozo Sh.CAA-4.Pe-1 (PEJERREY x-1), Cuenca del Colorado.
1023 Internal report. YPF Tecnología SA. pp. 17

1024 Ruiz, L., & Quattrocchio, M. (1997). Estudio palinológico de la Formación Pedro Luro
1025 (Maastrichtiano-Paleoceno) en la Cuenca del Colorado, República Argentina. Parte 1:
1026 Esporas y granos de polen. *Ameghiniana*, *34*(2), 115–137.

1027 Schreck, M., & Matthiessen, J. (2013). *Batiacasphaera micropapillata*:
1028 palaeobiogeographic distribution and palaecological implications of a critical Neogene
1029 species complex. In J. Lewis, F. Marret, & L. Bradley (Eds.), *Biological and Geological*
1030 *Perspectives of Dinoflagellates* (pp. 301–314). The Micropalaeontological Society,
1031 Special Publications, Geological Society, London.

Schreck, M., Matthiessen, J., & Head, M. J. (2012). A magnetostratigraphic calibration of middle Miocene through Pliocene dinoflagellate cyst and acritarch events in the Iceland Sea (Ocean Drilling Program Hole 907A). *Review of Palaeobotany and Palynology*, *187*, 66–94. https://doi.org/10.1016/j.revpalbo.2012.08.006

Schreck, M., Nam, S. I., Clotten, C., Fahl, K., De Schepper, S., Forwick, M., & Matthiessen, J. (2017). Neogene dinoflagellate cysts and acritarchs from the high northern latitudes and their relation to sea surface temperature. *Marine Micropaleontology*, *136*, 51–65. https://doi.org/10.1016/j.marmicro.2017.09.003

Shevenell, A. E., Kennett, J. P., & Lea, D. W. (2004). Middle Miocene southern ocean cooling and Antarctic cryosphere expansion. *Science*, *305*(5691), 1766–1770. https://doi.org/10.1126/science.1100061

Sluijs, A., Pross, J., & Brinkhuis, H. (2005). From greenhouse to icehouse; organic-walled dinoflagellate cysts as paleoenvironmental indicators in the Paleogene. *Earth-Science Reviews*, *68*(3-4), 281–315. https://doi.org/10.1016/j.earscirev.2004.06.001

Soliman, A. (2012). Lower and Middle Miocene dinoflagellate cysts from the Gulf of Suez and the Red Sea, Egypt. *Palaeontographica Abteilung B*, *287*(4-6), 95–139.

Strauss, C., & Lund, J. J. (1992). A Middle Miocene dinoflagellate cyst microflora from Papendorf near Hamburg, Germany. *Mitteilungen aus dem Geologisch-Paläontologischen Institut der Universität Hamburg*, *73*, 159–189.

Strauss, C., Lund, J. J., & Lund-Christensen, J. (2001). Miocene dinoflagellate cyst biostratigraphy of the Nieder Ochtenhausen research borehole (NW Germany). *Geologisches Jahrbuch A*, *152*, 395–447.

1054 Tyson, R. V. (1995). *Sedimentary Organic Matter: Organic Facies and Palynofacies*.
1055 Chapman & Hall.

1056 Uliana, M. A., & Biddle, K. T. (1988). Mesozoic-Cenozoic paleogeographic and
1057 geodynamic evolution of Southern South America. *Revista Brasileira de Geociências*,
1058 *18*(2), 172–190.

1059 Uchupi, E., & Emery, K. O. (1991). Pangaean divergent margins: historical perspective.
1060 *Marine Geology*, *102*(1-4), 1-28.

1061 Versteegh, G. J. M. (1994). Recognition of cyclic and non-cyclic environmental
1062 changes in the Mediterranean Pliocene: a palynological approach. *Marine*
1063 *Micropaleontology*, *23*(2), 147–183. https://doi.org/10.1016/0377-8398(94)90005-1

1064 Westerhold, T., Marwan, N., Drury, A. J., Liebrand, D., Agnini, C., Anagnostou, E., ...
1065 & Zachos, J. C. (2020). An astronomically dated record of Earth's climate and its
1066 predictability over the last 66 million years. *Science*, *369*(6509), 1383–1387.
1067 https://doi.org/10.1126/science.aba6853

1068 Williams, G. L., Brinkhuis, H., Pearce, M. A., Fensome, R. A., & Weegink, J. W.
1069 (2004). Southern Ocean and global dinoflagellate cyst events compared: index events
1070 for the Late Cretaceous–Neogene. *Proceedings of the Ocean Drilling Program,*
1071 *Scientific Results*, *189*, 1–98.

1072 Williams, G. L., Fensome, R. A., & MacRae, R. A. (2017). The Lentin and Williams
1073 index of fossil dinoflagellates 2017 edition. *AASP Contributions Series*, *48*, 1–1097.

1074 Wilson, G. J. (1973). Palynology of the middle Pleistocene Te Piki bed, Cape Runaway,
1075 New Zealand. *New Zealand Journal of Geology and Geophysics*, *16*(3), 345-354.

Zachos, J., Pagani, M., Sloan, L., Thomas, E., & Billups, K. (2001). Trends, rhythms, and aberrations in global climate 65 Ma to present. *Science*, *292*(5517), 686–693. https://doi.org/10.1126/science.1059412

Zavala, C., Abrameto, A., Azúa, G., Freije, H., Inchentronn, C. H., & Ponce, J. J. (2000). Estratigrafía de los acantilados marinos de la zona de El Cóndor-Bahía Rosa (Formación Río Negro, Mioceno-Plioceno). *Actas del II Congreso Latinoamericano de Sedimentología* (pp. 186–187).

Zevenboom, D. (1995). *Dinoflagellate cysts from the Mediterranean late Oligocene and Miocene* (Doctoral dissertation). Universiteit Utrecht, Faculteit Biologie.

Zonneveld, K. A., Marret, F., Versteegh, G. J., Bogus, K., Bonnet, S., Bouimetarhan, I., ... & Young, M. (2013). Atlas of modern dinoflagellate cyst distribution based on 2405 data points. *Review of Palaeobotany and Palynology*, *191*, 1-197.

Acknowledgments

The authors thank the Palynology Laboratory of INGEOSUR-CONICET for the processing of the samples, and YPF S.A. for granting access to the samples used in this study. We are also grateful to an anonymous reviewer and E. G. Ottone for their careful review and constructive comments, which significantly improved the manuscript. We also thank the Editor for their guidance and handling of this manuscript.

Figure captions

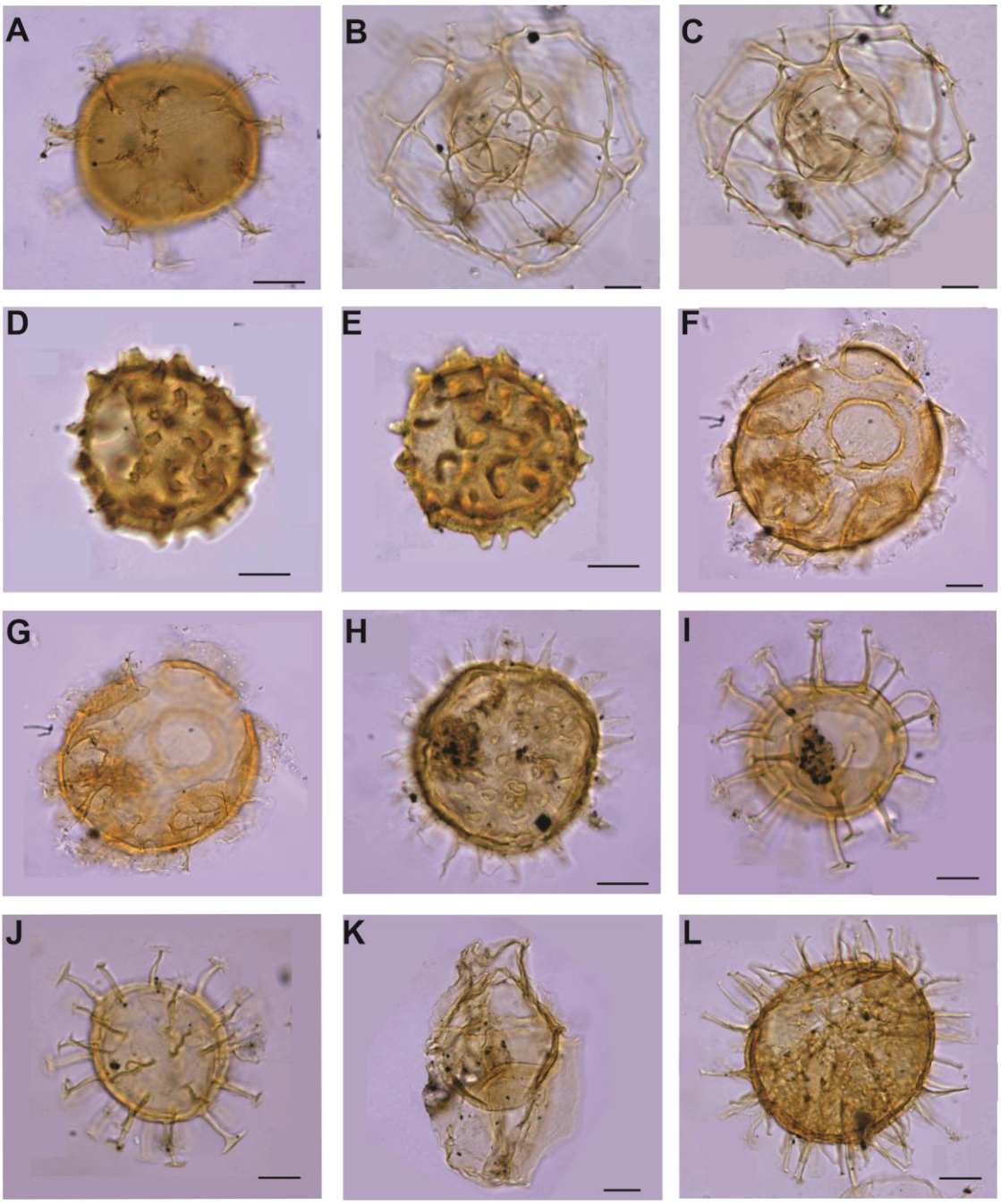


Figure 6. Dinoflagellate cysts from the Ranquel borehole section. A-Achomosphaera sp., general view; B, C- *Cannosphaeropsis quattrocchiae,* dorsal view*;* B, high focus; C, intermediate focus; D, E- *Cerebrocysta poulsenii*, ventral view*;* D, intermediate focus; E, high focus; F, G, *Cleistosphaeridium ancyreum,* apical view*;* F, intermediate focus; G, high focus. H- *Lingulodinium hemicystum*, dorsal view*;* intermediate focus; I, J- *Melitasphaeridium choanophorum,* dorsal view*;* I, intermediate focus, J, high focus; K-

Hystrichosphaeropsis obscura, dorsal view; L- *Operculodinium centrocarpum,* dorsal section. Scale bars = 10 µm.

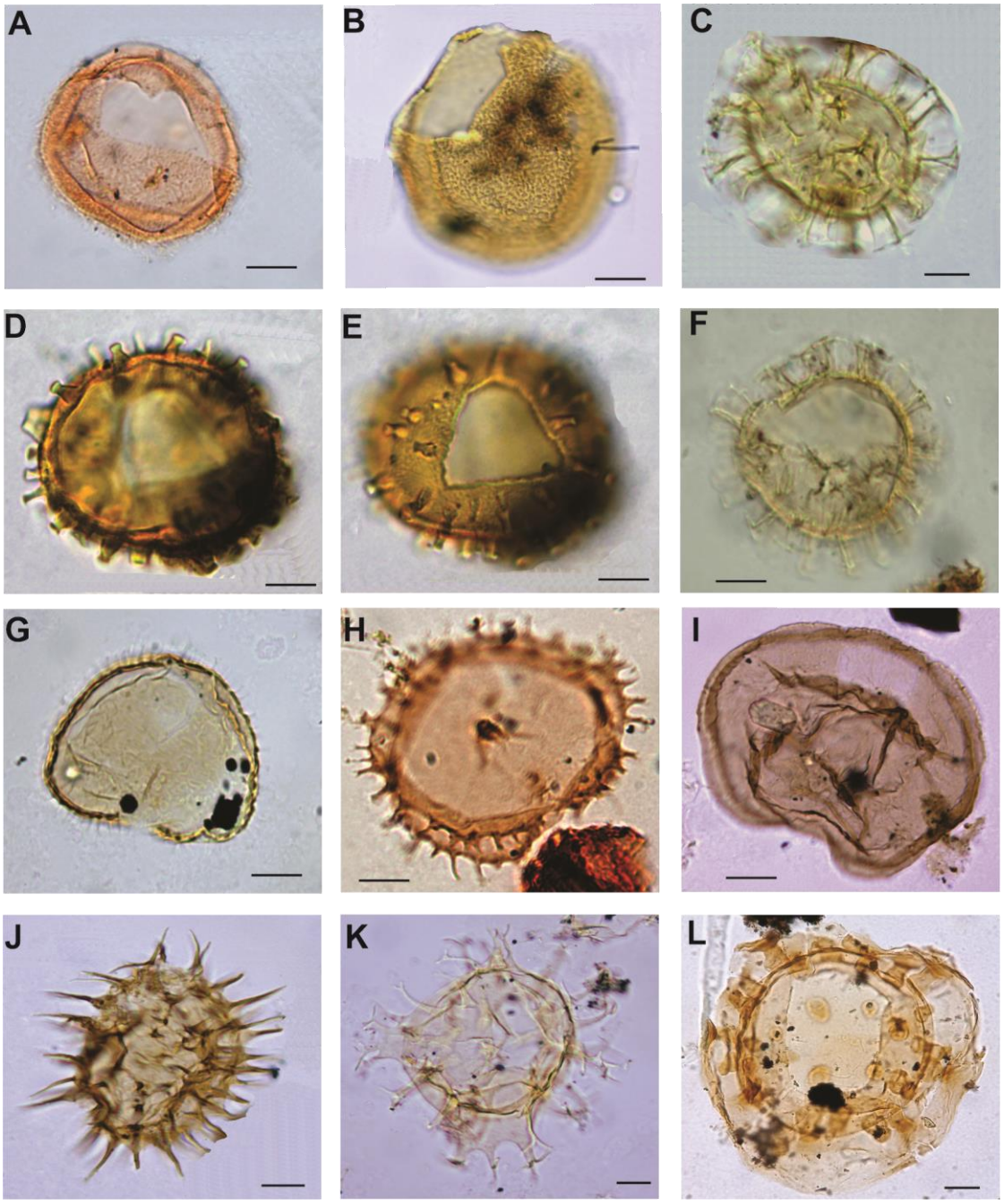


Figure 7. Dinoflagellate cysts from the Ranquel borehole section. A- *Bitectatodinium tepikiense,* dorsal view; B- *Cerebrocysta namonensis*, drosal view; C, F-, *Labyrinthodinium truncatum,* dorsal view*;* C, high focus; F, intermediate focus; D, E- *Operculodinium piaseckii,* dorsal view*;* D, low focus; E, high focus; G- *Selenopemphix brevispinosa*, apical view; H- *Selenopemphix dionaeacysta,* apical view; intermediate

focus; I- *Selenopemphix nephroides,* antapical view*;* intermediate focus; J- *Selenopemphix quanta,* dorsal view; K- *Spiniferites mirabilis,* dorsal view; L- *Tuberculodinium vancampoae,* dorsal view. Scale bars = 10 µm.

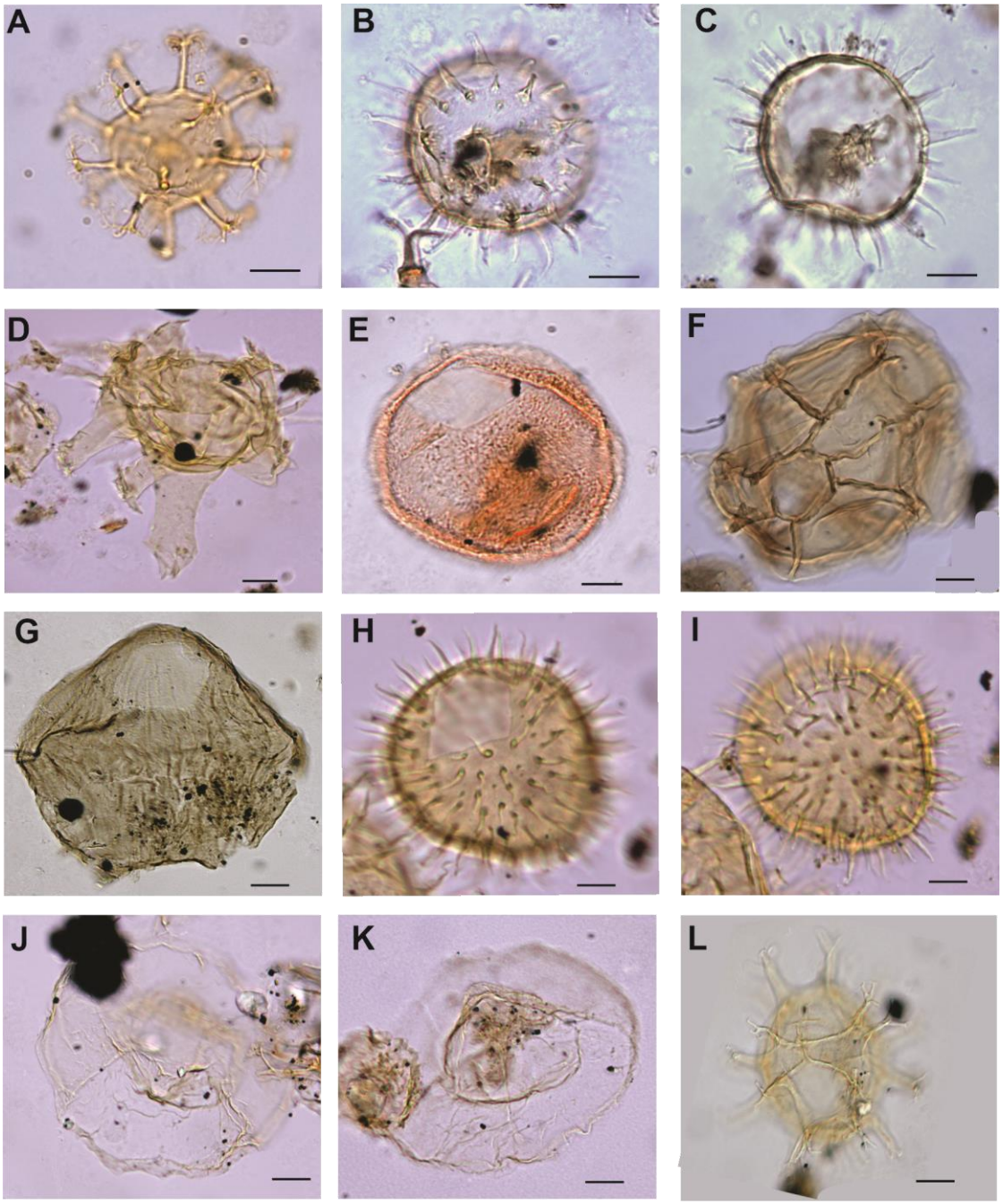


Figure 8. Dinoflagellate cysts from the Ranquel borehole section. A- *Reticulatosphaera actinocoronata,* dorsal view; B, C- *Dapsilidinium pseudocolligerum,* dorsal view*;* B, high focus; C, intermediate focus; D- *Hytrichokolpoma rigaudiae,* ventral view; E- *Habibacysta tectata*, ventral view*;* F- *Impagidinium* sp., dorsal view; G- *Lejeunecysta*

1117 sp., ventral view; H, I- *Operculodinium janduchenei,* ventral view; H, high focus; I,

1118 intermediate focus; J, K- *Saturnadinium* sp., apical view; L- *Spiniferites* sp. ventral view.

1119 Scale bars = 10 μm.

1120 **Appendix 1.** List of species mentioned in the text

1121 **Calcareous nannofossis**

1122 *Calcidiscus premacintyrei* Theodoridis, 1984

1123 *Chiasmolithus* sp. Hay, Mohler & Wade, 1966

1124 *Coccolithus pelagicus* (Wallich, 1877) Schiller, 1930

1125 *Cyclicargolithus floridanus* (Roth & Hay, 1967) Bukry, 1971

1126 *Reticulofenestra bisecta* (Hay, Mohler & Wade, 1966) Roth, 1970

1127 *Reticulofenestra dictyoda* (Deflandre, 1954) Stradner, 1961

1128 *Reticulofenestra lockeri* Müller, 1970

1129 *Reticulofenestra pseudoumbilicus* (Gartner, 1967) Gartner, 1969

1130 *Sphenolithus conicus* Bukry, 1971

1131 *Sphenolithus heteromorphus* Deflandre, 1953

1132 *Sphenolithus moriformis* (Brönnimann & Stradner, 1960) Bramlette & Wilcoxon, 1967

1133 **Dinocyst**

1134 *Achomosphaera sp.* (Fig. 6)

1135 *Algidasphaeridium sp.*

1136 *Batiacasphaera minuta* (Matsuoka, 1983) Matsuoka and Head, 1992

Bitectatodinium tepikiense Wilson, 1973 (Fig. 7)

Brigantedinium sp.

Cannosphaeropsis quattrocchiae (Guler et al., 2001) Guler et al., 2015 (Fig. 6)

Cerebrocysta namonensis Guler and Guerstein, 2013 (Fig. 7)

Cerebrocysta poulsenii de Verteuil and Norris, 1996 (Fig. 6)

Cleistosphaeridium ancyreum (Cookson and Eisenack, 1965) Eaton et al., 2001 (Fig. 6)

Dapsilidinium pseudocolligerum (Stover, 1977) Bujak et al., 1980 (Fig. 8)

Habibacysta tectata Head et al., 1989 (Fig. 8)

Hystrichokolpoma rigaudiae Deflandre and Cookson, 1955 (Fig. 8)

Hystrichosphaeropsis obscura Habib, 1972 (Fig. 6)

Impagidinium sp. (Fig. 8)

Labyrinthodinium truncatum Piasecki, 1980 (Fig. 7)

Lejeunecysta sp. (Fig. 8)

Lingulodinium hemicystum Matsuoka, 1983 (Fig. 6)

Melitasphaeridium choanophorum (Deflandre and Cookson, 1955) Harland and Hill, 1979 (Fig. 6)

Nematosphaeropsis rigida Wrenn, 1988

Operculodinium centrocarpum (Deflandre and Cookson, 1955) Wall, 1967 (Fig. 6)

Operculodinium eirikianum Head et al., 1989

Operculodinium janduchenei Head et al., 1989 (Fig. 8)

Operculodinium piaseckii Strauss and Lund, 1992 (Fig. 7)

Reticulatosphaera actinocoronata (Benedek, 1972) Bujak and Matsuoka, 1986 (Fig. 8)

Saturnadinium sp. (Fig. 8)

Selenopemphix brevispinosa Head et al., 1989 (Fig. 7)

Selenopemphix dionaeacysta Head et al., 1989 (Fig. 7)

Selenopemphix nephroides Benedek, 1972 (Fig. 7)

Selenopemphix quanta (Bradford, 1975) Matsuoka, 1985 (Fig. 7)

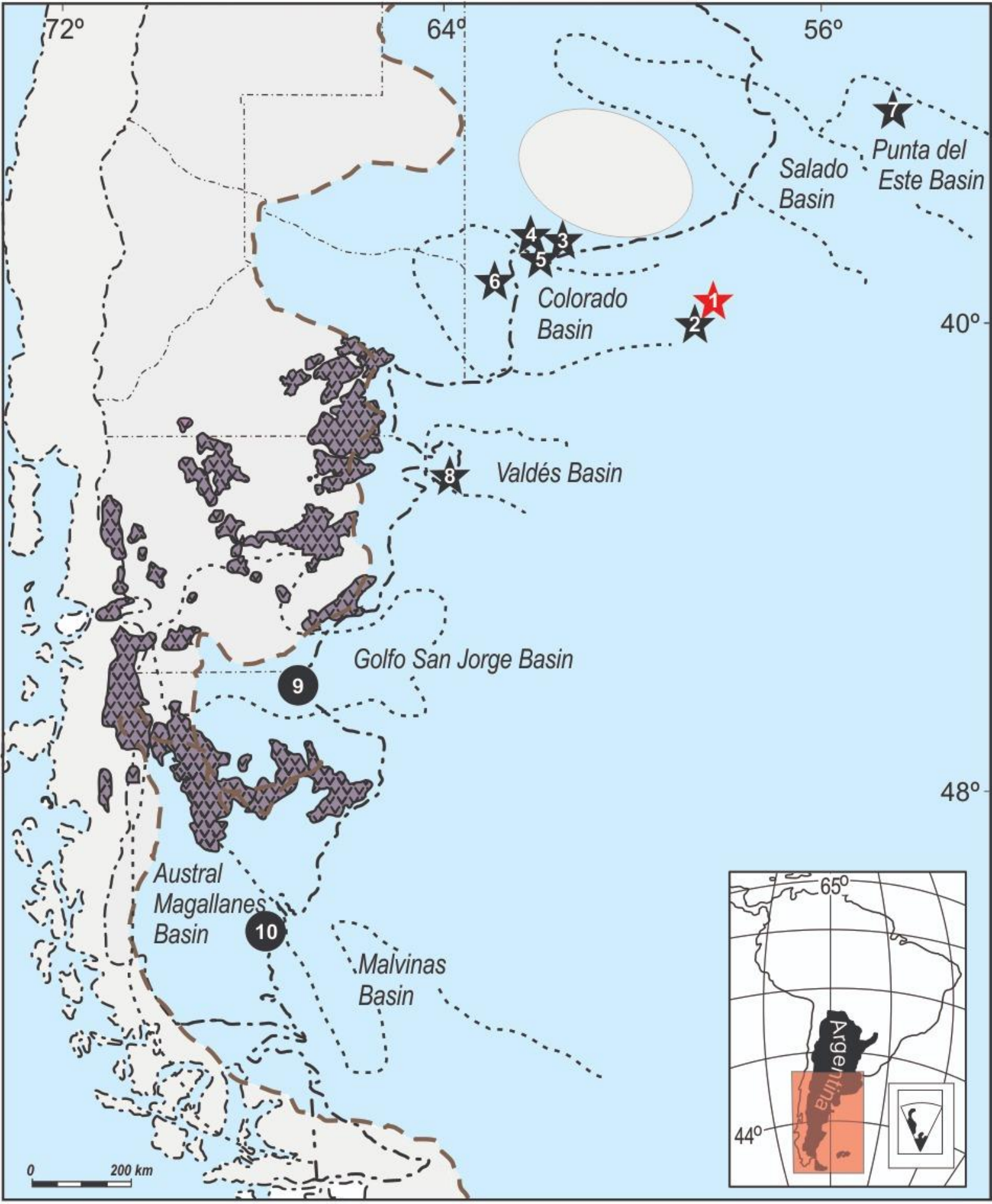
Spiniferites mirabilis (Rossignol, 1964) Sarjeant, 1970 (Fig. 7)

Spiniferites ramosus (Ehrenberg, 1838) Mantell, 1854

Spiniferites sp. (Fig. 8)

Trinovantedinium glorianum (Head et al., 1989) de Verteuil and Norris, 1992

Tuberculodinium vancampoae (Rossignol, 1962) Wall, 1967 (Fig. 7)



Chon Aike Province

Positive Areas.

Early to Middle Miocene Sea

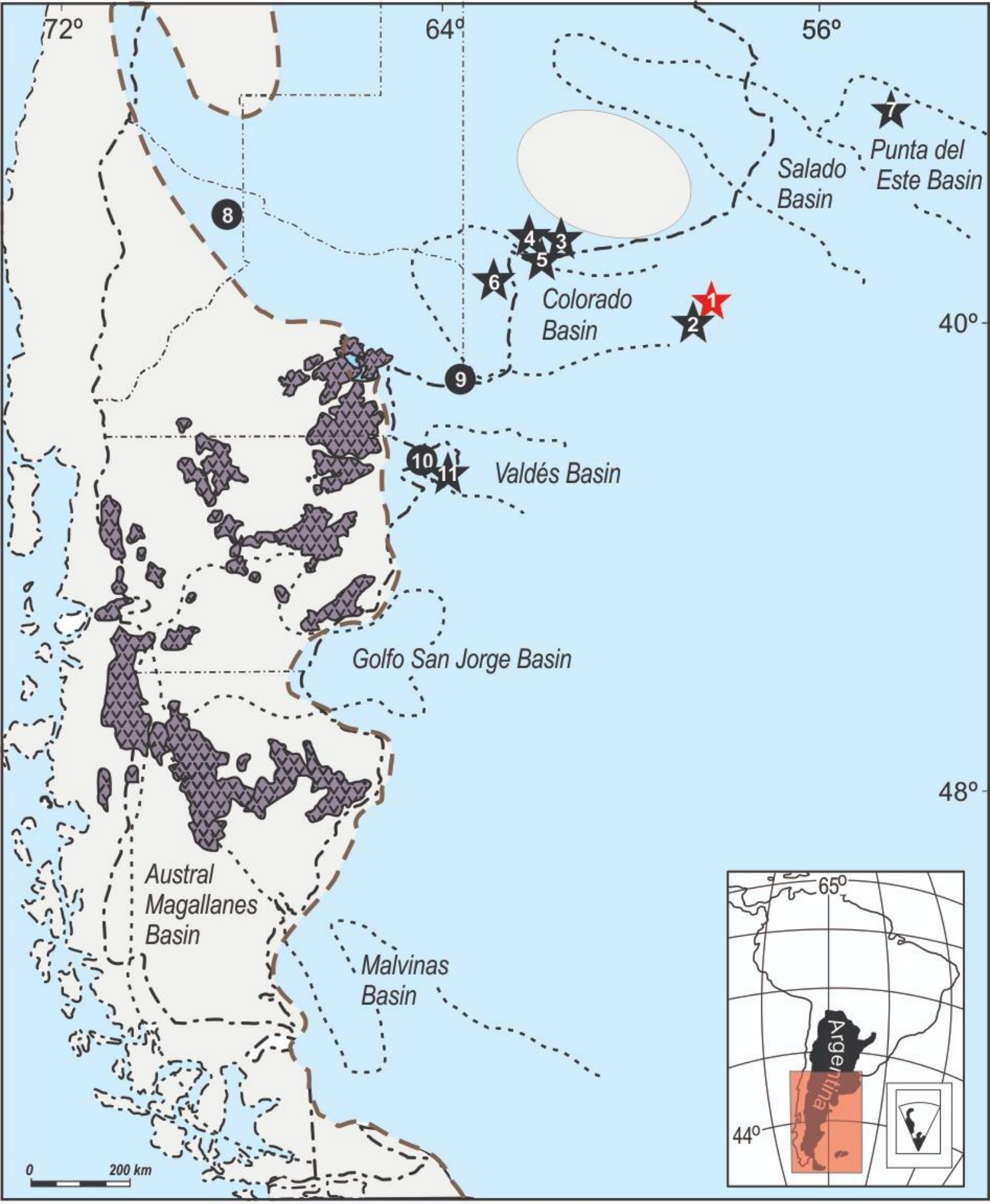
Basin Boundary

Estimated Paleocoastline

Boundary Country

2 Wells

9 Outcrops



Chon Aike Province

Middle to Late Miocene Sea

Estimated Paleocoastline

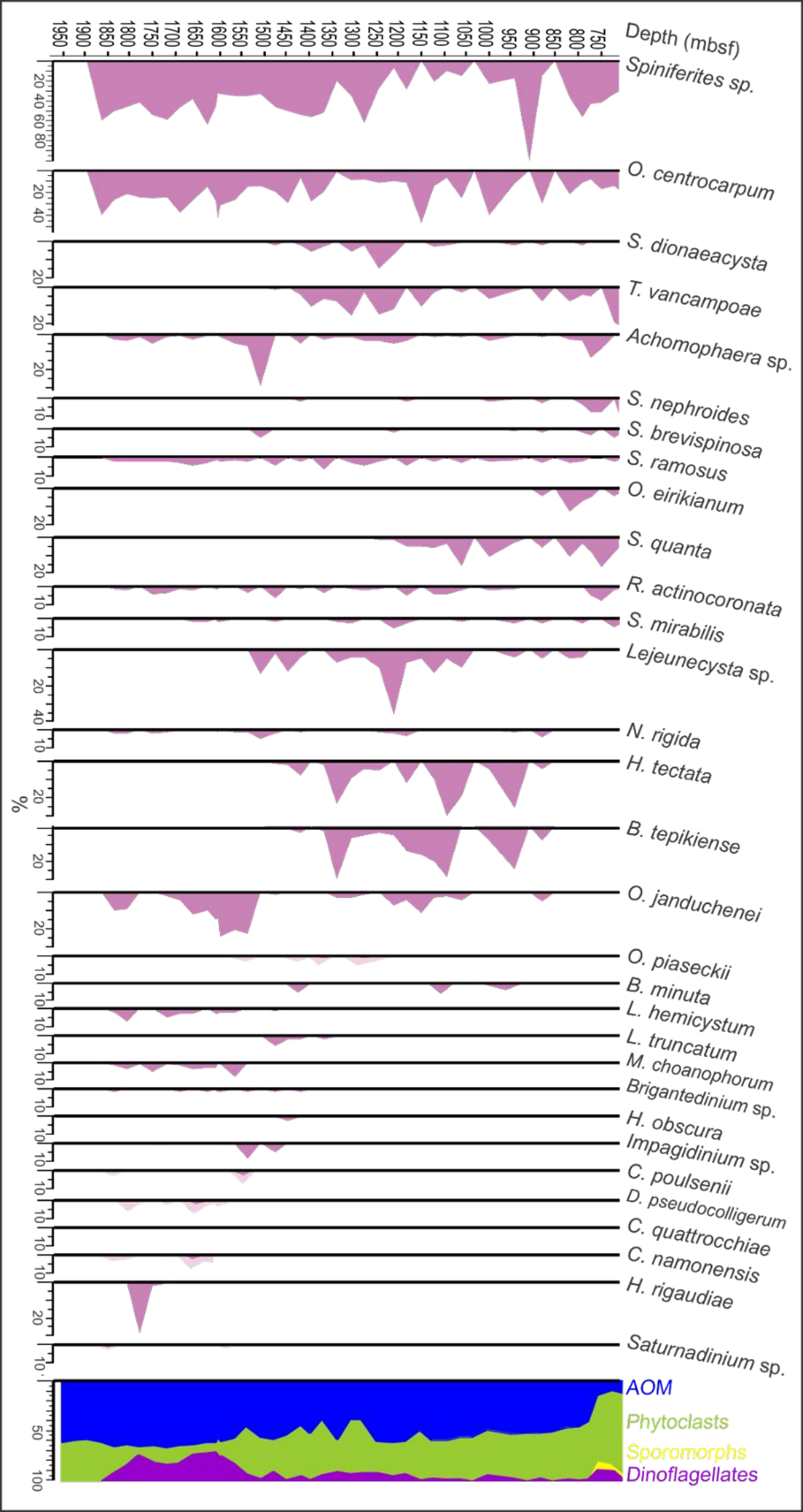
2 Wells

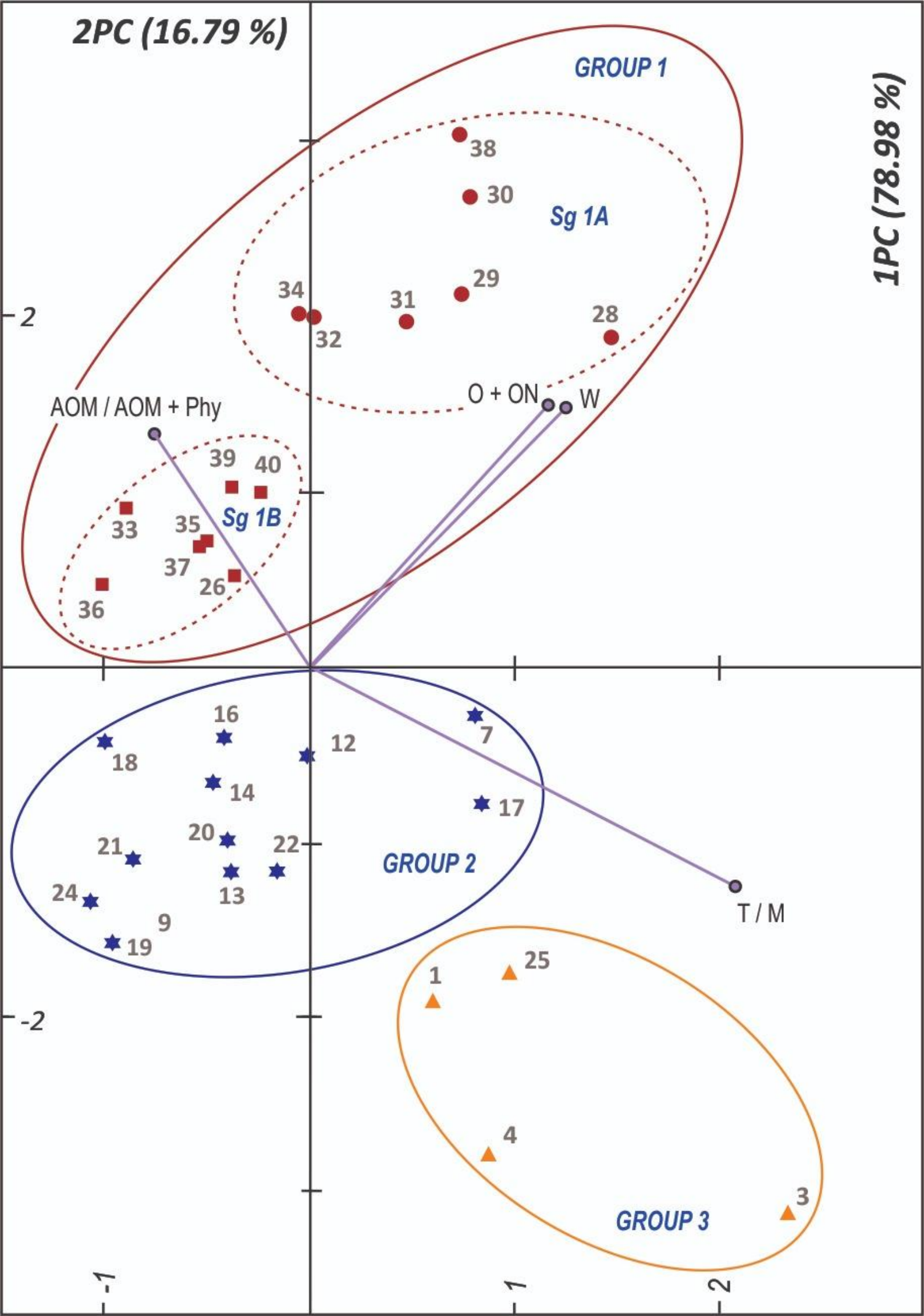
Positive Areas.

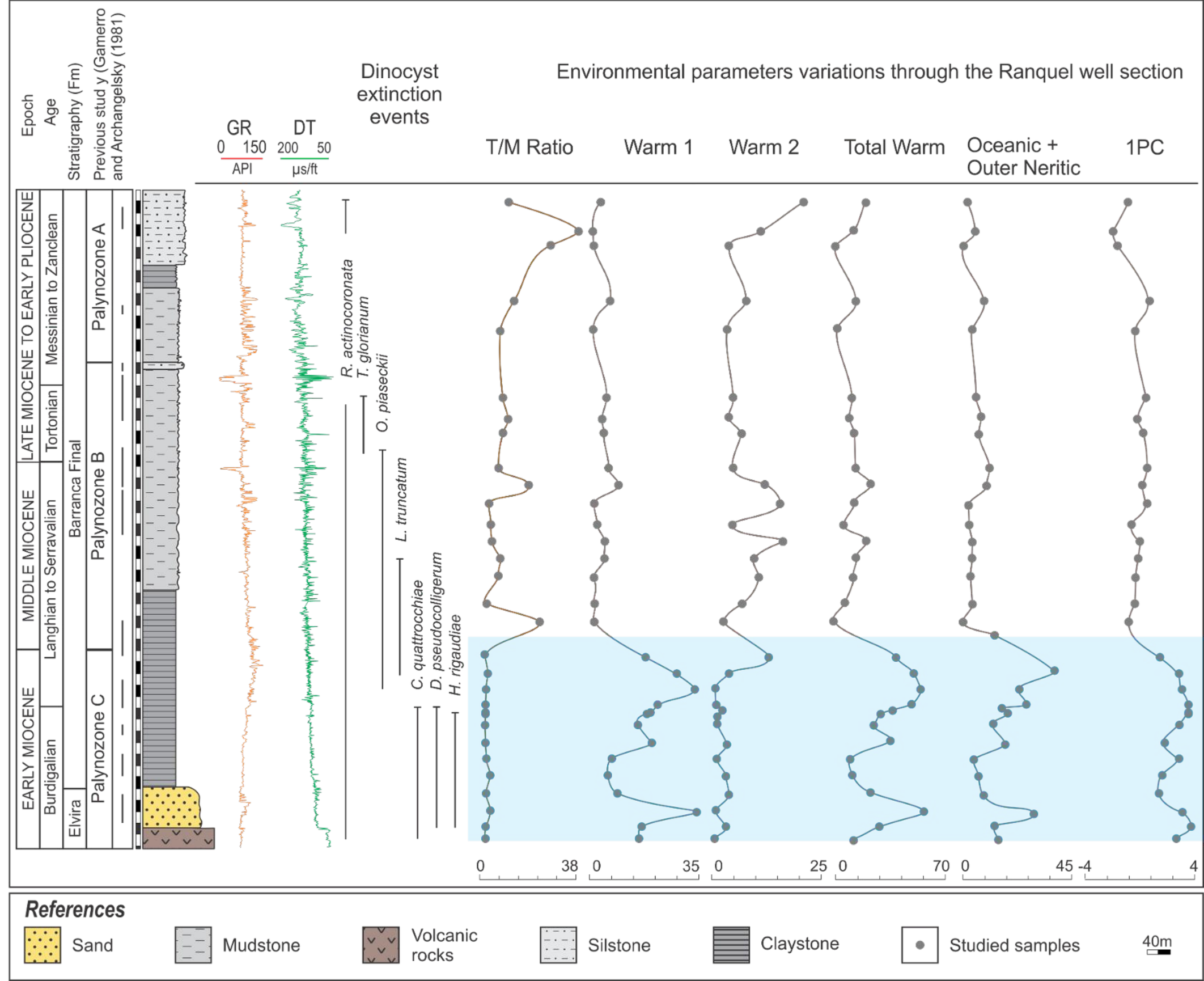
Basin Boundary

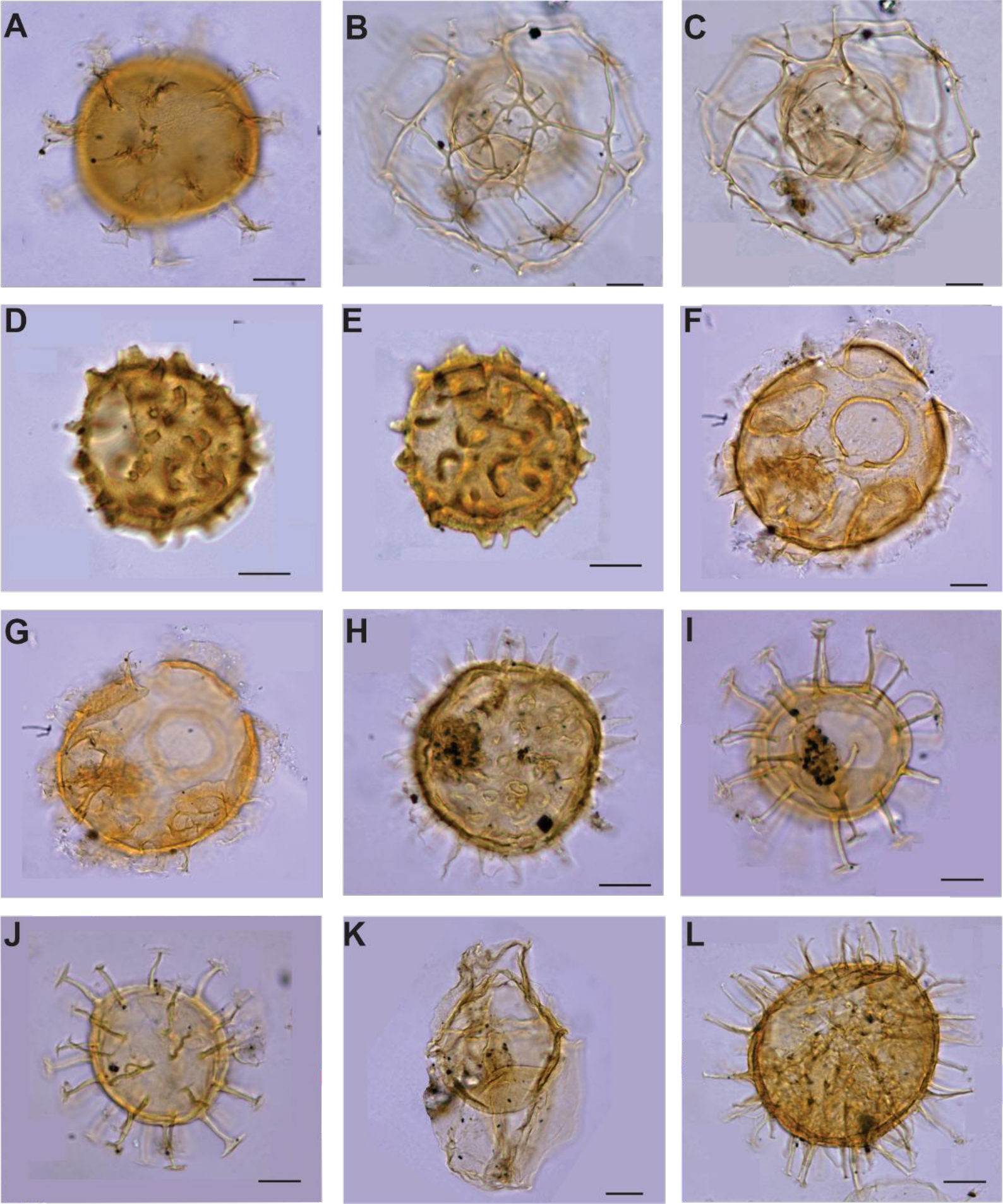
Boundary Country

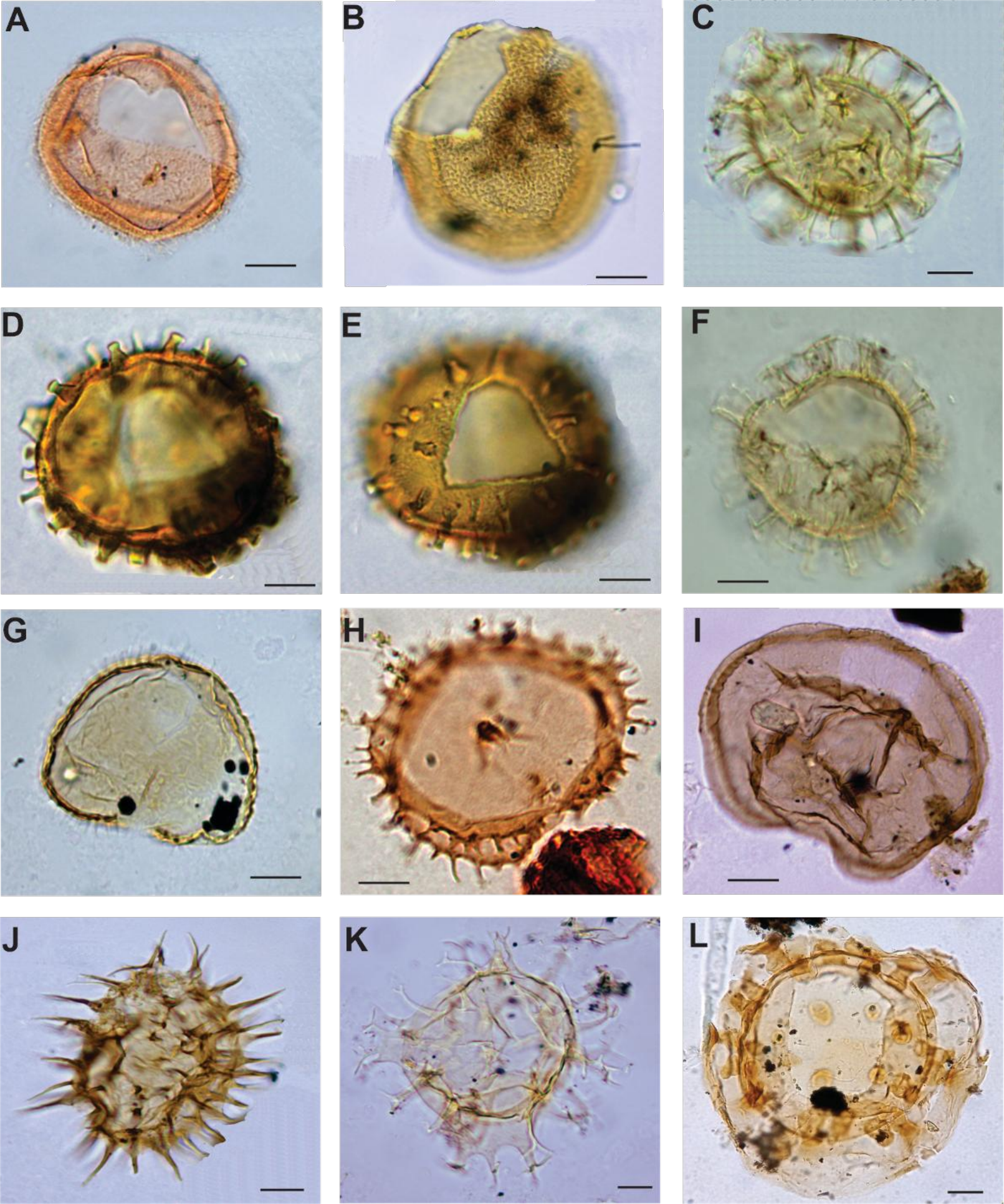
9 Outcrops

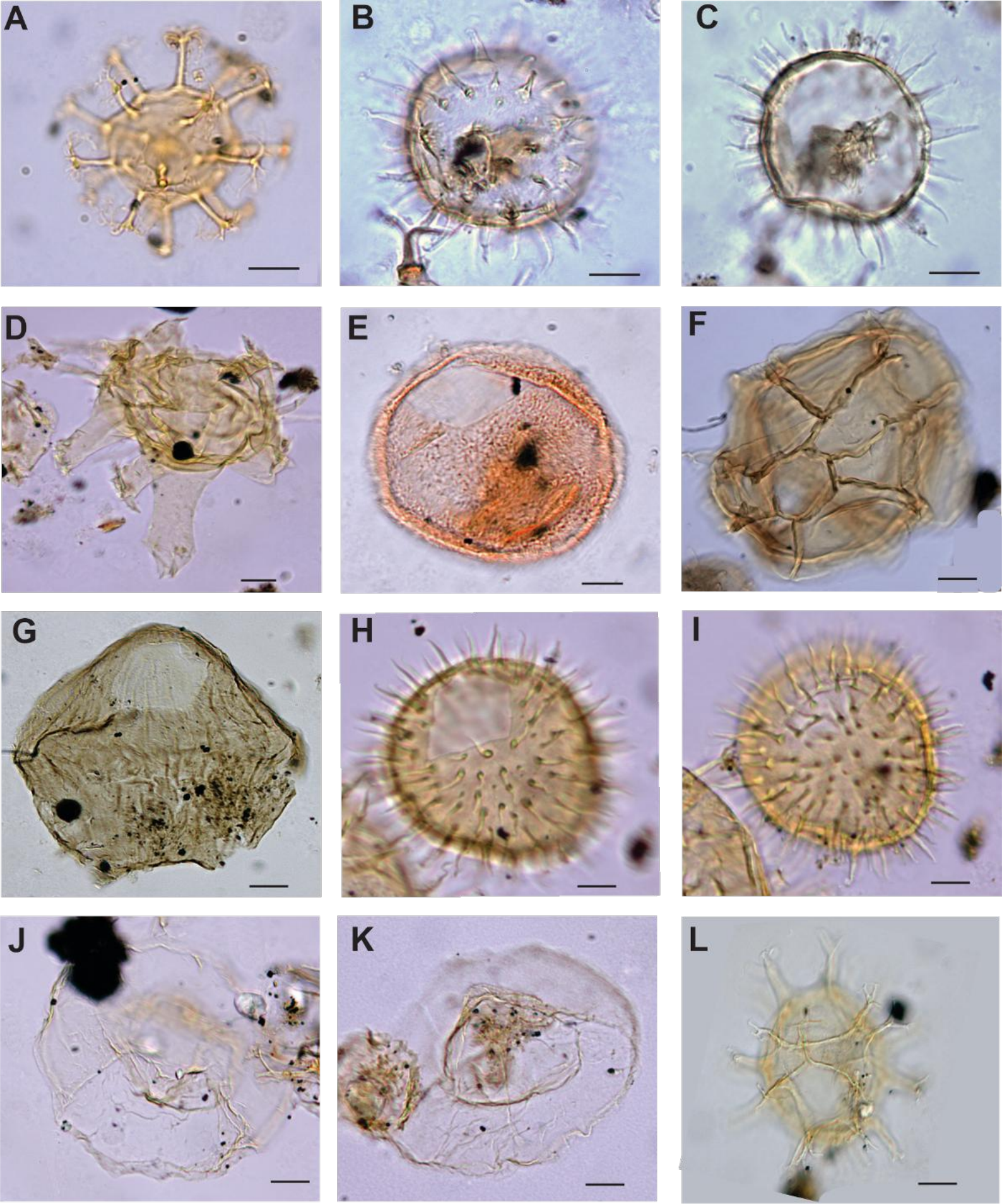

Depth (mbsf)
1950 1900 1850 1800 1750 1700 1650 1600 1550 1500 1450 1400 1350 1300 1250 1200 1150 1100 1050 1000 950 900 850 800 750
Spiniferites sp.
O. centrocarpum
S. dionaeacysta
T. vancampoae
Achomophaera sp.
S. nephroides
S. brevispinosa
S. ramosus
O. eirikianum
S. quanta
R. actinocoronata
S. mirabilis
Lejeunecysta sp.
N. rigida
H. tectata
B. tepikiense
O. janduchenei
O. piaseckii
B. minuta
L. hemicystum
L. truncatum
M. choanophorum
Brigantedinium sp.
H. obscura
Impagidinium sp.
C. poulsenii
D. pseudocolligerum
C. quattrocchiae
C. namonensis
H. rigaudiae
Saturnadinium sp.
%
AOM
Phytoclasts
Sporomorphs
Dinoflagellates


2PC (16.79 %)
1PC (78.98 %)
GROUP 1
Sg 1A
Sg 1B
GROUP 2
GROUP 3
38
30
29
34
31
32
28
39
40
33
35
37
26
36
AOM / AOM + Phy
O + ON
W
T / M
16
12
7
18
14
17
20
22
21
13
24
9
19
25
1
4
3
2
-2
-1
1
2


Epoch
Age
Stratigraphy (Fm)
Previous stud y (Gamerro and Archangelsky (1981)
GR
0 150
API
DT
200 50
µs/ft
Dinocyst extinction events
Environmental parameters variations through the Ranquel well section
T/M Ratio
Warm 1
Warm 2
Total Warm
Oceanic + Outer Neritic
1PC
EARLY MIOCENE
MIDDLE MIOCENE
LATE MIOCENE TO EARLY PLIOCENE
Burdigalian
Langhian to Serravalian
Tortonian
Messinian to Zanclean
Barranca Final
Elvira
Palynozone C
Palynozone B
Palynozone A
R. actinocoronata
T. glorianum
O. piaseckii
L. truncatum
C. quattrocchiae
D. pseudocolligerum
H. rigaudiae
0 38
0 35
0 25
0 70
0 45
-4 4
References
Sand
Mudstone
Volcanic rocks
Silstone
Claystone
Studied samples
40m


A
B
C
D
E
F
G
H
I
J
K
L


A
B
C
D
E
F
G
H
I
J
K
L


A
B
C
D
E
F
G
H
I
J
K
L